RPNSci
ISSN: 3006-8460 (Online)
3006-8452 (Print)

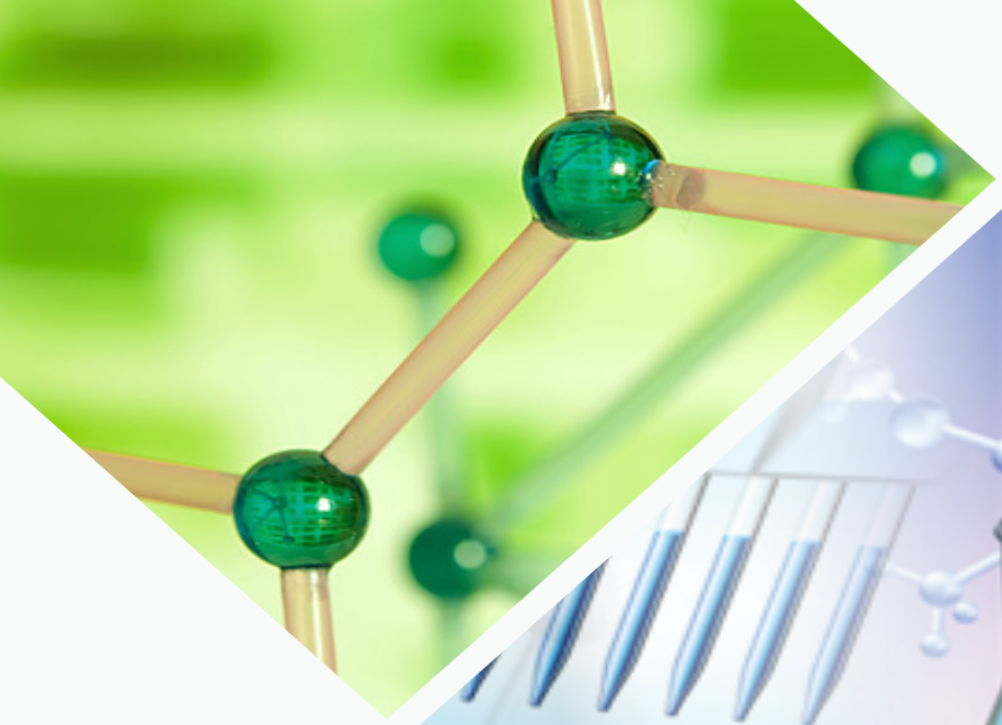

RESEARCH PROSPECTS IN NATURAL SCIENCES

VOLUME: 2
ISSUE: 2
2024

PUBLISHER
Government Graduate College, Township, Lahore

RESEARCH PROSPECTS IN NATURAL SCIENCES

Volume 2; Issue 2

Publisher: Government Graduate College, Township, LAHORE

Published by Government Graduate College, Township, Lahore.

Publication Data: December 2024

Research Prospects in Natural Sciences: A Research Journal
Printed in Lahore, Pakistan.

Contents

Available online at www.rpnsci.com

ISSN (P): 3006-8452, ISSN (O): 3006-8460

Research Prospects in Natural Sciences, Vol. 2, Issue 2, (2024) 1–12

Review Article

Role of hepatitis C virus envelope proteins in vaccine design

Areeba Maryam[a,*], Komal Fatima[a], Areeba But[a]

[a]*Department of Biomedical Engineering, University of Engineering and Technology Lahore, Narowal Campus, Pakistan*

Abstract

Hepatitis C virus (HCV) infection remains a significant global health problem, affecting millions of individuals with confirmed liver conditions. Despite recent advancements in antiviral therapies, the development of an effective Vaccine remains a top priority. Understanding the molecular epidemiology and viral evolution of hepatitis C virus (HCV) infection requires sequencing. Due in part to the tremendous genomic variety found in HCV, there is currently limited uniformity among sequencing methodologies. HCV envelope proteins, in particular E1 and E2, are critical targets for vaccine development because they play a critical role in the infection's entrance into host cells. These envelope proteins, particularly E1 and E2, are pivotal in facilitating the original intercourse between the virus and the host's vulnerable system, making them ideal targets for vaccine design. E1 and E2 are complex molecules with different structures, featuring glycosylation sites and containing essential antigenic regions that are critical for the host's vulnerable response. Still, their structural diversity poses a significant challenge in vaccine development. HCV is well- known for its inheritable variability, with multiple genotypes and quasi species circulating globally. This inheritable diversity has implications for the effectiveness of any potential vaccine, as a single strain may not give sufficient protection against the wide range of HCV variants. To address this challenge, innovative strategies are being explored. A general time-reversible substitution model was used to build phylogenetic trees, and sensitivity studies were carried out for each subregion.

Keywords:
Hepatitis C Virus, Antiviral Therapies, HCV Vaccine, Antigenic Regions, Conserved Epitopes

1. Introduction

Hepatitis C virus (HCV) was initially identified by Michael Houghton and associates in 1989 through cloning and sequencing of HCV genome collected from infected chimpanzees [1]. The virus is responsible for hepatitis C, which is an important global complaint chronically infecting around 57.8 million people. Hepatitis C virus significantly increases the incidence of health complications and fatality associated with liver diseases by elevating the chances of developing conditions such as liver cancer, cirrhosis, and liver fibrosis. Hepatitis C accounts for over 399,000 fatalities worldwide each year [2]. Patients typically acquire HCV through blood contact. Therefore, the highest risk groups consist of intravenous drug users, people who experienced blood transfusions before 1992, and healthcare professionals. Sexual transmission is now a significant problem among MSM who are HIV-positive, regardless of the fact that it is responsible for a very minor portion of the causes of acute hepatitis C. Seven to twenty-one days after the virus has been transmitted, HCV RNA can be found in serum. But prolonged incubation times can happen, particularly when only little virus loads have been transmitted [3].

The HCV symptoms starts to appear 3 to 12 weeks after exposure. The signs include fatigue, appetite loss, and jaundice. Serum alanine aminotransferase (ALT) levels rise within two to eight weeks of exposure, frequently exceeding the upper limits of the normal range. A week or two after exposure, serum can include HCV RNA. In the early weeks of infection, HCV RNA levels rise rapidly, reaching a peak between 105 and 107 IU/mL before the elevation of serum aminotransferase levels and the appearance of symptoms [4]. The majority of individuals with acute HCV infection approximately 80% to 85% fail to clear the virus and progress to chronic infection. Long-term persistence of the virus can result in serious complications, including cirrhosis, portal hypertension, hepatic decompensation with encephalopathy, and hepatocellular carcinoma [5].

2. Global Epidemiology

According to the World Health Organization (WHO), there are approximately 1.75 million new hepatitis C virus (HCV) in-

*Corresponding Author:
2020bme136@student.uet.edu.pk (Areeba Maryam)

fections annually, equating to a global incidence rate of 23.7 cases per 100,000 people. The Centers for Disease Control and Prevention (CDC) reported that hepatitis C-related deaths increased fourfold in 2020 compared to 2019. HCV prevalence varies significantly across different regions, ranging from 0.5% to 6.5%. In India, the reported prevalence is 0.9%, while it ranges from 0.5% to 1.5% in Western countries. Other regional estimates include 2.2% in Indonesia, 2.3% in Southeast Asia and Eastern Mediterranean regions, 6.5% in Pakistan, and 3.2% in China. WHO also estimates that 10 million people are living with chronic hepatitis C in the Western Pacific and Southeast Asia. Among Asian regions, Southeast Asia ranks just behind East Asia and South Asia in terms of HCV-related deaths [1].

The highest incidence is around 17.5% in Africa, 55.3% in Asia, 93.1% in the US, 88.1% in the Pacific, and 75.1% in Europe (Figure 1) [6]. Overall, it was projected that in 2019, there were 6.2 million new HCV infections, 540,000 HCVrelated deaths, and 15.3 million DALYs (disability-adjusted life years) associated with HCV, these figures represent increases of 25.4,59.1, and 43.6, respectively, from 1990. Men and women both have equal numbers of new HCV infections globally in 2019, but men endured more deaths and disability- adjusted life years (DALYs), as well as a bigger increase, than women. India and China were the two countries where nearly one-sixth of all new infections around the world started. India had the most DALYs connected to HCV infection among the three countries (India, China, and the United States), despite China having the most HCV infection-related mortality. Men had higher rates of incidence, fatalities, and DALYs than women in all three nations [7].

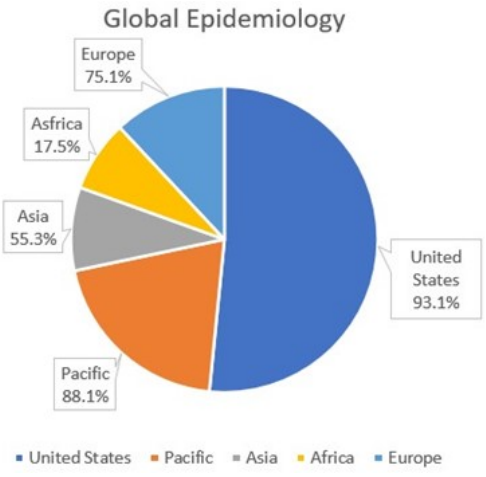

Figure 1: The highest frequency is around 17.5% in Africa 55.3% in, Asia , the 93.1% in US, 88.1% in the pacific , and 75.1% in Europe

In Pakistan the epidemiology of the hepatitis C virus was 16.47% in the general population, this study includes 765,426 individuals. While 8.2% in blood benefactors which covers the total 973,260 individuals. The average frequency in pregnant women (136,546) was 9.3%. This demonstrates that the prevalence of Hepatitis C was 11.32 percent in the general population, pregnant women, and blood benefactors [8].

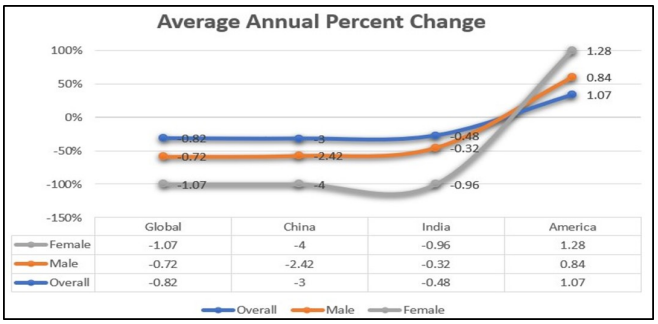

Figure 2: Age-standardized mortality rate (ASMR), average annual percent change (AAPC) from 1990 to 2019

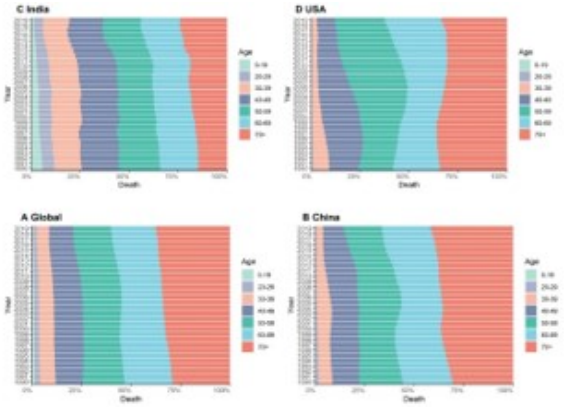

Figure 3: Age-specific HCV-related death rates by area from 1990 to 2019 (a) Global (b) China (c) India (d) The United States [7]

The age standardized incidence rate of the HCV infection (ASIR) worldwide in 2019 was 82.5 per 100,000 people, with a 95% confidence interval spanning 73.4 to 94.7. With a 95% UI range of 5.9 to 7.5, the age standardized mortality rate (ASMR) was 6.7 per 100,000 people. The age standardized delay rate (ASDR), with a 95% UI range from 160.7 to 210.2, was 184.5 per 100,000 people.

The average annual percent changes (AAPCs) for these three measures were, respectively, -0.30, -0.82, and -0.95 from 1990 to 2019. India's ASDR (Age Standardized Death Rate) was comparable to the global average. Age Standardized Incidence Rate (ASIR) was greatest in the United States and lowest in China. The Age Standardized Mortality Rate (ASMR) and Age Standardized Death Rate (ASDR) of the United States had the largest rise ratio among the three countries. For the United States, these values were 1.28 and 1.30, respectively. On the other side, China has seen a dramatic decline in the disease burden of HCV, especially among women. Among the three nations, Chinese women saw the biggest drops in ASDR and ASMR for HCV infection.. The corresponding AAPCs for Chinese women were -4.00 and 4.35, respectively [7].

People over the age of 70 accounted for more than 30% of HCV-related deaths worldwide, in China, and in the US in

2019. Among them, the United States' expanding population mortality rate is more pronounced, with a higher percentage of people in the 50 to 69 age group than in the rest of the globe, China, and India, as shown in (Figure 3).In India, the age distribution of the death rate is sufficiently balanced. Therefore, those who were 70 years of age or older suffered the greatest number of Hepatitis C virus-related deaths worldwide. The average annual percent changes (AAPCs) for these three measures were, respectively, -0.30, -0.82, and -0.95 from 1990 to 2019. India's ASDR (Age-Standardized Death Rate) was comparable to the global average. The Age-Standardized Incidence Rate (ASIR) was greatest in the United States and lowest in China. The Age Standardized Mortality Rate (ASMR) and Age Standardized Death Rate (ASDR) of the United States had the largest rise ratio among the three countries. For the United States, these values were 1.28 and 1.30, respectively. On the other side, China has seen a dramatic decline in the disease burden of HCV, especially among women. Among the three nations, Chinese women saw the biggest drops in ASDR and ASMR for HCV infection. The corresponding AAPCs for Chinese women were -4.00 and 4.35, respectively. (Yang, Qi et al. 2023). People over the age of 70 accounted for more than 30% of HCV-related deaths worldwide, in China, and in the US in 2019. Among them, the United States' expanding population mortality rate is more pronounced, with a higher percentage of people in the 50 to 69 age group than in the rest of the globe, China, and India, as shown in (Figure 3).In India, the age distribution of the death rate is sufficiently balanced. Therefore, those who were 70 years of age or older suffered the greatest number of Hepatitis C virus-related deaths worldwide.

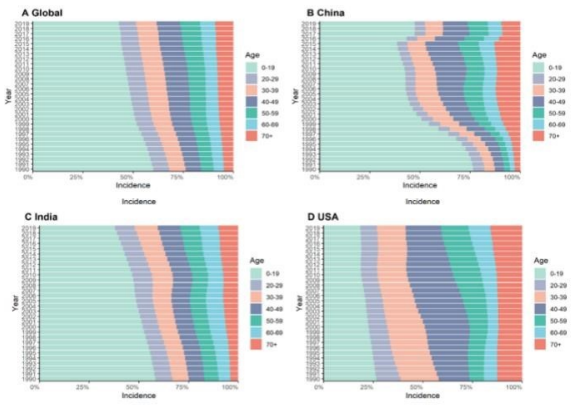

Figure 4: (A) Global (B) China (C) India (D) The United States (Constitution of incidence due to HCV by age groups in different areas from 1990 to 2019 [7]

3. Mode of Transmission

The Hepatitis C virus spreads through blood borne, perinatal, and sexual channels; however, the virus is not transferred through breastmilk, feces, or informal interactions [9].The most efficient way for HCV to spread is by prolonged or frequent direct percutaneous exposure, much like with blood transfusions and other blood products, organ transplants from contagious donors, and needle sharing among injection drug users (IDU). HCV can also spread by parenteral exposure, prenatal exposure, sexual contact, domestic contact, and parenteral exposure in a medical context. Although transmission through other unproven sources, such as contaminated instruments used in public health campaigns, traditional drugs like acupuncture, open folk drugs, tattooing, body piercing, and marketable barbering, has not been proven in the USA, similar routes may be crucial in sustaining the spread of HCV in some areas of Asia [10]. In the latter half of the 20th century, the hepatitis C virus (HCV) infection spread quickly due to the widespread availability of injectable medicines and the rise in the use of illicit injection drugs. The main risk factors for HCV transmission globally have been iatrogenic exposures and the use of illicit injectable therapies. Unsafe corrective injection procedures tend to be the leading cause of infections in underdeveloped nations. Donor testing has almost completely eliminated transfusion-related illnesses in developed nations, but infections spread to patients via improper injection procedures are a growing issue. The main risk factor for HCV is injection drug use; prevalence is still high among new injectors, and this likely explains or obscures the connections between HCV-positive people and histories of noninjecting drug use, tattooing, and incarceration. Increased use of illicit drugs may contribute to the rise in sexually transmitted HCV infections among HIV-positive men who engage in male sex [11].

4. HCV Genome

The diameter of the positive stranded, single stranded, spherical, enveloped hepatitis C virus (HCV) is between 40 and 80 nm. This virus belongs to the Flaviviridae family and is categorized under the Hepacivirus genus. The 9.6 kb HCV genome encodes a single polyprotein that is broken into ten mature proteins by cellular and viral enzymes [12]. Previous research has shown that the HCV genome is abundant in complex RNA structures, comprising useful RNA motifs in both the coding and untranslated regions (UTRs). One of the best-characterized IRES structures in any system is found within the 5´ UTR of the HCV, for instance. It is known that the core region of HCV contains highly conserved substructures, many of which are engaged in long-range interactions that are crucial for viral replication and translation [13].

With icosahedral symmetry, the nucleocapsid is made up of multiple copies of the core proteins and genomic RNA. A host cell-derived lipid bilayer envelope with the envelope glycoproteins E1 and E2 incorporated surrounds the nucleocapsid (Figure 5). Major protein components of the virion include the core protein and the E1 and E2 envelope glycoproteins. The virus's genome, which contains about 9600 nucleotides, is converted into a single precursor protein with 3020 amino acids. A large open reading frame (ORF) and highly conserved 5´ UTR and 3´ TR sections are both present in the genome. There are structural and nonstructural proteins in the HCV genome [14]. The HCV genome shows non-homogenous mutation rates throughout. It was discovered that substitution biases are largely

different between two nearby genomic regions and depend on the nucleotide composition of the genome [15].

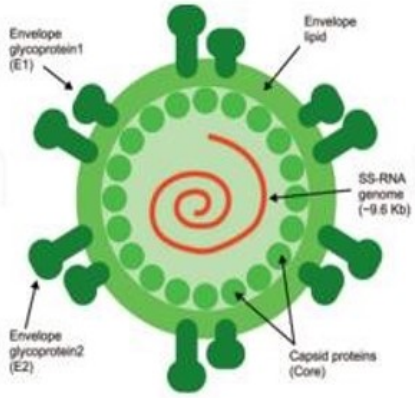

Figure 5: The Hepatitis C Virus has a single stranded, positive sense RNA molecule for its genome. It belongs to the Hepaciviral genus and the Flaviviridae family. The 9.6 kilobases (kb)-long HCV genome encodes a single polyprotein that is later degraded into separate proteins [14]. One ORF that encodes a polyprotein covers the majority of HCV genome. Viral and host proteases repurpose this polyprotein into distinct viral proteins. These proteins contain nonstructural proteins (NS1, NS2, NS3, NS4A, NS4B, NS5A, and NS5B) as well as structural proteins (Core, E1, and E2)

5. HCV Genotypes

HCV is divided into number of various genotypes and subtypes due to its genetic variability. For the accurate diagnosis, effective management, and treatment of HCV infections, it is essential to comprehend these genotypes. There are many subtypes for each of the HCV's seven main genotypes that are Genotype 1 (GT1), Genotype 2 (GT2), Genotype 3 (GT3), Genotype 4 (GT4), Genotype 5 (GT5), Genotype 6 (GT6) and Genotype 7 (GT7). It's crucial to remember that HCV genotypes can affect how the disease develops, the antiviral medications that are used, and the possibility that a given treatment will be effective. All genotypes now have considerably higher cure rates thanks to improvements in HCV therapy; however, each genotype may require a different treatment plan and time frame. The understanding of HCV genotypes is still developing, and additional genotypes and subtypes may be discovered in the future.

6. HCV Genotypes Pervalence

Understanding the distribution of HCV genotype prevalence by geographical location is crucial for developing efficient strategies for diagnosis, treatment, and prevention. There are 86 different sub-genotypes and 8 genotypes of HCV throughout the world. Because the RNA-dependent RNA polymerase (RdRp) lacks a proofreading mechanism, it is a very error-prone enzyme, leading to a significant degree of sequence variability in the freshly replicated HCV genomes. Most HCVassociated liver infections are caused by genotypes 1, 2, and 3, which are widespread worldwide and account for 90% of all infections. It is important to remember that genotypes with a global distribution are unevenly represented in various geographical areas. In the United States, Europe, Japan, and Australia, genotype 1 is more common. Genotype 3 is frequent in India, Pakistan, and Afghanistan, while genotype 2 is more common in South America, China, and Japan [16]. The most widespread genotype worldwide is GT1, which is especially prominent in North America, Europe, and Australia. While subtype 1b is more prevalent in Europe, subtype 1a is more prevalent in North America. According to a 2016 study that appeared in the Journal of Hepatology, subtype 1a of HCV was more widespread in the US and was the most common genotype among individuals with chronic infections [17]. Although GT2 is less frequent than GT1, it may still be found in many places throughout the world, including North America, Europe, and Asia. Those of subtypes 2a and 2b are more prevalent. GT2 is rather widespread in Japan. According to a 2016 study that appeared in the Journal of Gastroenterology, patients with chronic HCV were most likely to have the GT2 genotype.

South Asia, Southeast Asia, and several regions of Europe are home to GT3. GT3 is frequently linked to more severe liver disease. The most common genotype of HCV infection in India was GT3, according to a 2015 study that was published in the Journal of Medical Virology [18]. Particularly in Egypt, GT4 is widely used in the North Africa and Middle East ,the most prevalent subtype is 4a. Due mostly to GT4 infections, Egypt has among the most prevalent rates of HCV in the world. The predominance of GT4 in Egypt was described in a study that was published in the Journal of Infectious Diseases in 2008 [19]. Genotype 5 is a somewhat uncommon variant that is mostly found in a few places, with South Africa being one of these locations. Although GT5 has been found in various countries, including France, it is still primarily concentrated in South Africa. The most prevalent form of GT5 is subtype 5a [20]. Southeast Asian nations like Vietnam, Thailand, Cambodia, Laos, and Myanmar are predominantly home to the genotype 6. With varying subtype distribution, it is one of the most common genotypes in the area. The most prevalent subtype of GT6 is 6a [21]. The Hepatitis C Virus (HCV) genotype 7 (GT7) has not been generally identified or thoroughly researched. More research is required to completely understand the distribution of GT7, which is mostly prevalent in Central Africa [22].

According to recent study in Pakistan in 2023, Genotype 3 was found to be the predominant genotype, accounting for 93.75% of the samples. Other genotypes were detected at lower frequencies, with genotype 1 representing 3.25% of the samples, genotype 2 and genotype 4 each representing 1.25% of the samples. None of the samples included genotypes 5 or 6, which were undetectable. A total of 0.5% of the samples contained two recombinant Hepatitis C strains. Although one

sample could not be typed, it was found to have a genotype 3 variation. The analysis of the baseline data showed that 51.0% of the samples were of the male gender. The participants were 43 years old on average. The viral load ranged from 2x103 to 1x107 U/mL, while the mean ALTs levels were 105 U/L. In 2021, a study was conducted in Tehsil Babozi, District Swat of province Khyber Pakhtun Khaw of Pakistan, to investigate the prevalence of Hepatitis C Virus (HCV) in the population. The total population of the study area was 278,401, and a sample of 223 individuals was taken from a different site within the area [23].

The research involved both males and females to determine the gender-wise prevalence of HCV. Out of the 223 individuals analyzed, 169 were males and 53 were females. The study found that the prevalence of HCV in males was 1.78%, while in females it was 5.66%. This indicates that females were more infected with HCV compared to males. The higher prevalence of HCV in females may be attributed to factors such as lack of awareness about HCV, lower levels of education, and non-compliance with prescribed medications. Another study conducted on HCV prevalence found no statistically significant difference between males and females or between different locations. However, it revealed that there were more male patients with HCV compared to females. The highest prevalence was observed in men with a rate of 4%, while in females, the prevalence was relatively low at 1.1%. This study also indicated a higher occurrence of HCV contamination in older individuals.

The individuals included in the study ranged in age from 17 to 82, with an average age of 37 years. All patients tested positive for HCV antibodies, indicating an infection. The likelihood trends were somewhat greater among males in all age categories, but there was no statistically significant gender difference in the occurrence of HCV infection. In conclusion, women were more likely than men to have HCV in the research area. To investigate the underlying causes of this gender gap in HCV infection, more study is necessary [23]. The samples were also collected from individuals belonging to various age groups. The study included both males and females, who were divided into different age categories, such as 15-15, 16-25, 26-35, and so on, up to 105. The prevalence of HCV was found to be 1.6% in the 15-26 age group, 1.05% in the 26-35 age group, 2.7% in the 36-45 age group, 4% in the 46-55 age group, and 6.25% in the 56-65 age group. The results indicated that there is a higher prevalence of HCV in older individuals above the age of 50. This may be due to a weakened immune response to the pathogen and other agerelated diseases.

Furthermore, the results showed a statistically significant increase in the likelihood of anti-HCV prevalence with increasing age. Another study conducted on HCV prevalence found that HCV was very rare in patients aged 15 years or below, while a higher frequency of HCV was observed in older age groups. According to a survey on several age groups, the 20 to 29-year-old age range had the highest occurrence. A decline in the prevalence of active HCV was seen in age groups older than 40. According to the findings of the study, out of a total of 223 individuals, 1289 (57.4%) had no history of viral infection, while 94 (42.2%) had been affected by viral infection in the past. Among the 94 individuals with a history of viral infection, 2.12% tested positive for HCV, indicating a relationship between HCV infection and past viral infection [23]. The study also analyzed information from patients with longlasting viral hepatitis. It was discovered that patients with longlasting hepatitis B had much higher secondary, hospital, management, and overall incomes than did hepatitis B virus carriers and patients with long-lasting hepatitis C [16].

An interesting approach for the management of severe HCV and the prevention of chronic hepatitis has been proposed. Some scientific and legal actions have suggested that treating hepatitis C infection during the acute stage is associated with a high rate of sustained virological response, ranging from 75% to 100%. However, while there is a general consensus that intervention during the acute stage improves viral clearance, there are still unanswered medical questions and uncertainties regarding the optimal treatment for severe hepatitis C infection and the documentation of sustained virological response (SVR) outcomes [16]. The first significant factor in the fixed model was the patient's age, which showed a positive significance. This indicates that with an increase of 1 year in the patient's age, the risk of hepatitis C infection will increase by 1.035 times, assuming all other factors remain constant. As a one-year increase does not result in a significant change, the change was examined after 20 years. This suggested that with a 20-year increase in age, the risk of Hepatitis C disease doubles. HCV occurrence was found to be directly related to age, meaning that the older the age, the higher the occurrence of HCV [23].

7. HVC Glycoproteins

The hepatitis C virus (HCV) glycoproteins E1 and E2 are the most important targets for neutralizing antibodies. This is a direct result of their roles in mediating the virus's entry into susceptible cells, which is pH- and clathrinid-dependent. The N-terminal portion of the HCV genome houses the two genes that produce the glycoproteins. After the glycoproteins are initially made as a part of the viral polyprotein, the host cellular proteinases signal peptidase and signal peptide peptidase release the mature proteins. The mature, cleaved E1 protein has 192 amino acids, while the E2 protein has 363-369 amino acids, depending on the viral strain. The connections between the transmembrane domains of the glycoproteins, which each chaperon the folding of the other during synthesis, cause them to form heterodimers [24]. The fact that amino acid variation in the E1 and E2 proteins between infectious primary isolates exceeds 37% emphasizes the enormous genetic diversity that the E1 and E2 genes are capable of tolerating. The E2 protein's three hypervariable regions (HVRs) have the highest level of amino acid variety. The HCV polyprotein's HVR1, a region of 26-27 amino acids at the very end of E2, has the most variability. Compared to the HVR2, the intergenotypic variable region (IgVR) is situated nearer to the E2 transmembrane domain and CD81 binding regions. Despite this difference, both proteins exhibit extensive glycosylation on their surfaces as well as conserved N- and O-linked glycans. As the primary receptor binding protein, E2 interacts with the cell surface molecules CD81,

SR-BI, and occluding. While the interaction with SR-BI is assumed to be controlled by the N-terminal hypervariable region (HVR1) of the E2 protein, the binding surface between E2 and CD81 is a discontinuous surface containing three highly conserved areas of the E2 protein. It has been widely documented how E2 and cell surface receptors interact. The main result of neutralizing Abs is probably to prevent receptor interactions [25].

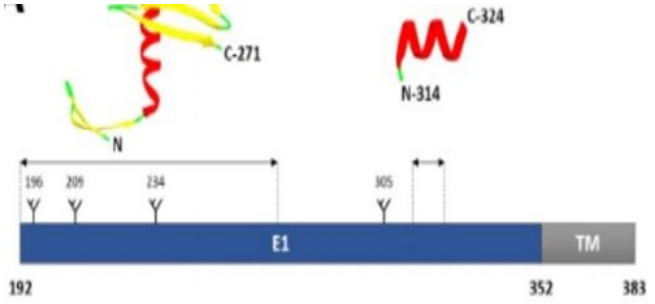

Figure 6: HCV E1 (aa192-383) in a linear diagram, along with the crystal structures of its segments aa192-271 (PDB: 4UOI) and aa314324 (PDB: 4N0Y)[25]

8. Structure of E1

The E1 glycoprotein is one of the two HCV envelope glycoproteins; the other is E2. In the early stages of HCV infection, these glycoproteins work together quite effectively. The viral envelope must fuse with the cell membrane in order for the virus to enter and infect the host cell, and E1 is essential for mediating this process. This procedure, which is also a key target for antiviral medications, is necessary for the development of HCV infection. The structure of E1 is characterized by a number of distinctive characteristics that allow it to carry out its crucial tasks during HCV infection. E1 is a type I transmembrane protein, which means that it spans and is anchored within the viral lipid envelope. The hydrophobic amino acid residues in this transmembrane region enable E1 to bind to the viral membrane. Because it is a crucial part of the viral envelope, E1 is excellently positioned for its role in aiding the fusion of the viral envelope with the host cell membrane [26].

E1 has two primary extracellular domains, E1a and E1b, which interact with host factors when the virus is infected and are visible on the viral surface. The initial attachment of the virus to the host cell surface is caused by the E1a domain. E1a has regions that interact with co-receptors and host cell receptors, making it easier for HCV to bind to the cell. The process of fusion involves E1b. Once the virus is linked to the host cell, E1b interacts with E2 and other viral and host components to induce fusion, finally allowing the viral genetic material to enter the host cell. E1 and E2 work together in the early stages of HCV infection. E1's function increases during the fusion process, whereas E2 is principally in charge of the virus's attachment to host cell receptors. The heterodimeric complex that E1 and E2 create improves their capacity to mediate viral entry.

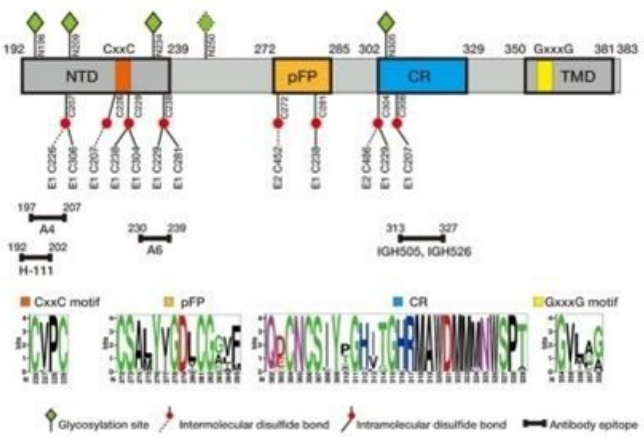

Figure 7: Hepatitis C virus (HCV) E1 envelope protein-schematic diagram [27]

The specific areas and residues within E1 and E2 that interact with each other have been the subject of intense investigation to understand how they collaborate in the infection process [24].

E1 experiences post-translational changes, like many glycoproteins. The correct folding and operation of the protein depend on these changes, which include glycosylation. E1's conformation can be impacted by glycosylation, which may also contribute to immune evasion. It's crucial to comprehend the particular glycosylation patterns of E1 in order to design vaccines and target treatments. The genetic heterogeneity of HCV is well documented, and this genetic variability extends to the E1 protein. The E1 sequences of different genotypes and subtypes of HCV differ. The effectiveness of viral entrance, the immunological response, and even the susceptibility to antiviral therapy can all be affected by this genetic variation. In order to comprehend HCV epidemiology and create individualized treatment plans, researchers explore these genetic variations in E1.

9. Functions of E1

The HCV E1 glycoprotein's actions are crucial for the virus's capacity to infect host cells and start an infection. E1 is involved in the early phases of HCV's life cycle, including host cell adhesion and membrane fusion. For the creation of antiviral treatments and vaccines to prevent HCV infections, it is essential to comprehend the roles of E1. E1a's main function is to aid in the virus's initial attachment to host cells. The first stage in establishing an HCV infection is this connection. The virus can attach to the surface of the host cell thanks to E1a's interaction with particular co-receptors and host cell receptors. E1a interacts with host cell receptors such as CD81 and class B type I scavenger receptors (SR-B1). The interaction between E1a and CD81 is essential for HCV entrance and is required for the virus to cling to host cells. Co-receptors like claudin-1 and occluding are also involved in the attachment process in addition to receptors. Viral binding to host cells is further made possible by interactions between E1a and these co-receptors [28].

Due to the genetic diversity of HCV, different genotypes and subtypes have different E1 sequences. The effectiveness of viral attachment and penetration into host cells may be impacted by this heterogeneity. The viral envelope and the membrane of the host cell are fused predominantly by E1b. For the virus to transmit its genetic material into the host cell and start the infection, this fusion process is necessary. Early on in viral entry, E1, the first major envelope glycoprotein, collaborates with E2, the second major glycoprotein. While E2 is mainly responsible for binding to receptors, E1 and E2 interact to generate a heterodimeric complex that improves the effectiveness of viral entry [29].

On going research is being done to determine how E1b mediates membrane fusion. For the purpose of creating ways to prevent viral entrance and hinder fusion, understanding this mechanism is essential. E1 is a major target in the development of vaccines because it has areas that potentially cause neutralizing antibodies. The objective is to create vaccinations that encourage the synthesis of antibodies that can neutralize HCV and stop infection [30]. Due to the virus's genetic diversity, which includes variance in E1 sequences among various genotypes and subtypes, developing an effective HCV vaccine is difficult. To guarantee widespread protection, vaccine candidates must take into account this variability [31].

10. Structure of E2

E2 protein is the second most significant glycoprotein of HCV which is characterized as type 1 transmembrane protein. It is comprised of 363 amino acids ranging from viral polyprotein position 384 to 746 [32]. It has a C terminal transmembrane domain and a N terminal ectodomain. The intensive post-translational changes that the E2 protein goes through include the creation of 9 to 11 N linked glycosylation sites and the presence of 18 cysteine residues that are conserved across all genotypes. These alterations are necessary for both immune infiltration and appropriate protein folding [33].

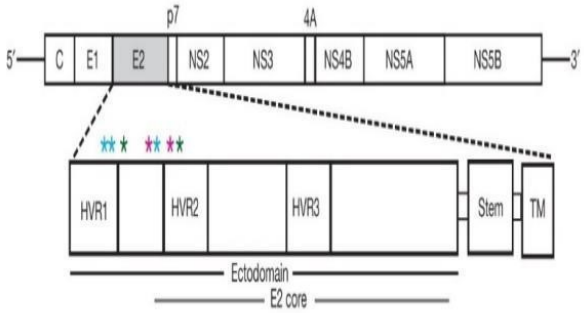

Figure 8: Organization of HCV genome and E2 protein. The HCV genome demonstrates the capsid protein (C), E1 protein and the structural proteins (NS2, NS3, NS4B, NS5A and NS5B). The grey bar indicates E2 core structure while black [33]

The structural analysis of E2 core reveals its packed globular structure with eight disulfide bonds and is highly glycosylated. The secondary structure of E2 core primarily comprises of β sheets and random coils with two small α helix [34].

The E2 core structure exhibits a sandwich of two anti-parallel β sheets (A and B) present at the center. These both front and back anti-parallel sheets are held together by disulfide bonds and intensively hydrophobic core. Sheet A undergoes an IgG like fold while the B sheet constitutes a novel fold [35].

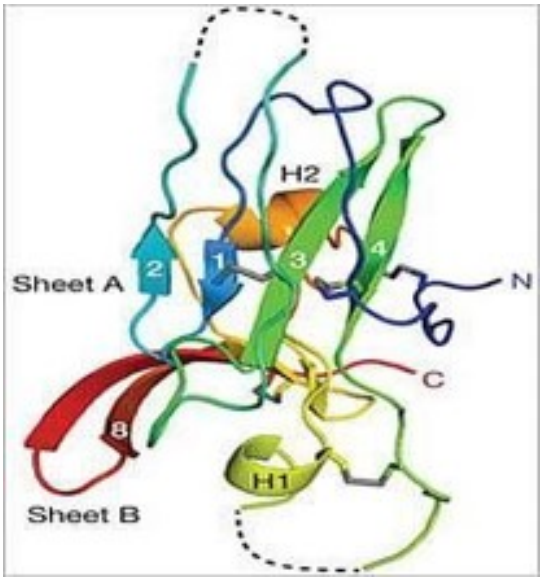

Figure 9: Representation of E2 core domain exhibiting the folding of sheets A and B [33]

11. Hyper Variable Region

The unmitigated genetic diversity of E2 proteins is exhibited through amino acid variations of more than 37% in among various primary isolates of HCV . The E2 protein comprises of three regions of immense variation of amino acids termed as Hyper Variable Regions(HRV). These include HVR1 (384-411), HVR2 (461-481), HVR3 (431-466), and IgVR (570-580) [36]. This diversity attributes to the mechanisms eluding the host immune system. Regardless of this extreme genetic variability in these proteins, there are regions of highly conserved genomic sequence regions exhibiting the N and O linked glycans and high surface glycosylation [37].

HRV1 exhibits the most diverse nature among all hyper variable regions and is located at N terminal ectodomain of E2 with a length of 26-27 amino acids ranging from 384 to 411 [38]. Due to its ability to maintain a certain shape and positively charged amino acid residues, HVR1 is essential for target cell identification and virus attachment [39]. HVR1 serves as a critical mediator in the initial stages of the HCV lifecycle, enhancing viral attachment to hepatocytes. This is largely due to its role in fostering interactions between the virus and various cellular receptors, particularly the scavenger receptor class B type

I (SR-BI) and low-density lipoprotein receptor (LDL-R). Intriguingly, HVR1´s interaction with low density lipo-protein receptor (LDL-R) may involve Apolipoprotein E (ApoE), a component of lipoproteins [40]. Consequently, specific antibodies targeting ApoE can effectively neutralize wild-type HCV particles, making HVR1 a prime significant factor in viral entry and propagation.

HVR1 contains epitopes for neutralizing antibodies and act as a prime target for vaccine formation. Its high sequence variability often compels the virus to mutate, allowing it to dodge the host's immune system [40]. Anti-HVR1 antibodies can disrupt the binding of broadly neutralizing antibodies to HCV, which is a significant aspect of the virus's evasion strategy. The other significant hyper variable region of envelope protein E2 of HCV is HVR 2 comprising of nine amino acids from polyprotein position 705 to 715 and is present down stream the HVR1. While HVR2 may not be the primary target for neutralizing antibodies, it plays a prime role in HCV's entry into host cells. It acts as alliance with HVR1 to influence interactions with key cellular receptors, such as CD81, which play significant role in the viral entry process [41]. The deletion of HVR2 or IgVR regions of E2 protein in HCV disrupts the formation of heterodimers between E1 and E2, which are indispensable for the virus's entry into host cells. This deletion significantly reduces HCV's binding to CD81, a critical host receptor required for successful entry [42]. Another important region exhibiting the high sequence variability in E2 protein is Immunoglobulin Variable Region also known as IgVR [43]. This is located further downstream of the HVR2 near the transmembrane domain of E2. IgVR complements HVR1 and HVR2 in the context of E2, further contributing to the HCV entry process. Similar to HVR2, IgVR does not seem to be the primary target for neutralizing antibodies. However, its absence, when deleted along with HVR2, disrupts the formation of E1E2 heterodimers, thereby affecting viral entry. Certain antibodies raised against the cytosolic portion of E2 exhibit increased reactivity towards E2. These antibodies display heightened effectiveness in reducing the interactions between E2 and CD81 when any of the hypervariable regions are deleted [40]. Of particular interest, some of these antibodies demonstrate remarkable broad neutralization capabilities across all HCV genotypes and are capable of recognizing epitope I. Deleting two or more hypervariable regions enhances their proficiency in inhibiting E2-CD81 interactions.

12. Functions of E2

The HCV E2 protein interacts with the other Envelope glycoprotein E1 to form a heterodimer, which is the main protein that helps the virus enter cells and fuse with other viruses. These two proteins are stabilized by disulfide connections and form bigger units with covalent bonding [44]. The lipid membrane produced by the host cells is injected into this E1-E2 protein heterodimer, which together with other components makes up the HCV envelope.

For cell surface molecules like CD81 and SR-BI, E2 protein serves as the primary receptor binding site [39]. The interaction of the Cd81 receptor binding site with the discontinuous surrounding surface of the three highly conserved areas of the HCV E2 protein serves as a metaphor for the binding reaction of E2 protein with Cd81 cell surface receptors [42]. The interaction between the SR-BI receptors and the N terminal hypervariable regions (HRV1) of the E2 protein is assumed to provide the basis for the binding response of E2 protein with the SR-BI [36].

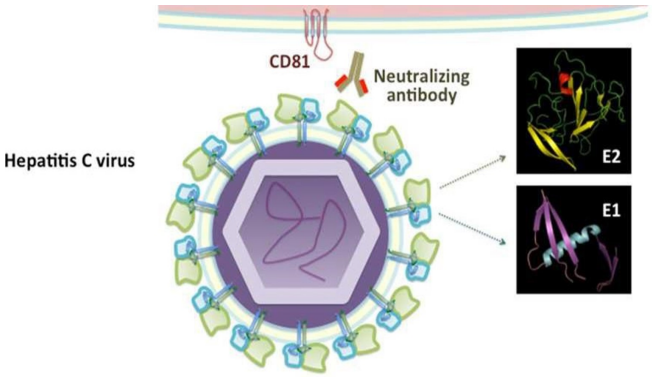

Figure 10: Model of the hepatitis C virus that shows how the E1E2 heterodimers are embedded in the lipid layer on the envelope [41]

13. Role of E1 and E2 in Development of Vaccine Against HCV

Various researches suggest E2 region as the most suitable target for developing a vaccine against HCV because it initiates humoral and cell mediated responses in humans [39]. However due to intensive mutating and genetically varying nature of HCV this task becomes tricky and remains unachievable. E1 and E2 play crucial roles in determining viral pathogenicity and influencing the host immune response, highlighting the significant potential of envelope glycoproteins in the development of a vaccine. Notably, the administration of a prime-boost regimen involving E1/E2 has been shown to induce cross-reactive immune responses in the chimpanzee model, resulting in the production of neutralizing antibodies. This finding suggests the presence of conserved immunogenic epitopes across different genotypes. According to recent studies, the administration of E1/E2 recombinant proteins to human volunteers has yielded the production of cross-neutralizing antibodies capable of targeting all significant genotypes. This outcome serves as a foundation for the advancement of a vaccine, utilizing the recombinant glycoproteins. Since the E2 protein region of HCV contains the most genetically diverse and varying sequences of amino acids, therefore the studies related to this protein will contribute to vaccine development [41]. E2 gains significant attention as the more immunogenic of the two envelope proteins. This is evident from the wealth of monoclonal antibodies raised against E2. In contrast, E1 is relatively less immunogenic during natural infections. Studies of the monoclonal antibodies targeting E1 are less common. However, experiments involving

E1 immunization do generate antibodies [45]. Chronic HCV infections may lead to the production of antibodies recognizing a conserved epitope within the E1 protein, specifically in the amino acid region between aa313-327 [46]. While prior vaccine candidates had limited success, future prospects hinge on eliciting broadly neutralizing antibodies (bnAbs) and an efficient T-cell response. Notably, bnAbs, specifically targeting conserved regions on E1 and E2, offer a promising avenue for vaccine design [47]. However, the structural flexibility of E1 and E2 epitopes presents challenges in vaccine development, necessitating a detailed understanding of their conformational changes during infection [48]. Significant strides have been made in the creation of a vaccine thanks to the HCV glycoproteins' architecture. However, the utilization of E2 alone for vaccine or medication design creates issues given that the majority of the E2 protein is made up of loops and flexible regions. A crucial neutralizing immunodominant face of the protein, the area between HVR-1 and HVR-2, which contains a portion of the AR3C epitope, appears to have substantial structural flexibility. The structural data for the broadly neutralizing AR3C antibody, however, is quite helpful. In addition, because the E2 core keeps its natural fold even after the HVR-1 and HVR-2 are removed, it's possible that future vaccine candidates will forgo including variable regions while still keeping the natural fold.

14. Phylogenetic Analysis

With the exception of Balochistan, where the most prevalent subtype is 1a, frequency research in 2013 showed that the most prevalent HCV genotype in Pakistan is 3a [49].The HCV glycoproteins (E1 and E2), which are hypervariable transmembranes found on the surface of the virus, are among its structural proteins and are crucial for the virus's attachment to the host cell via cell receptors. The C terminal sphere of envelope protein E1 is implicated in changes to membrane permeability and membrane association.

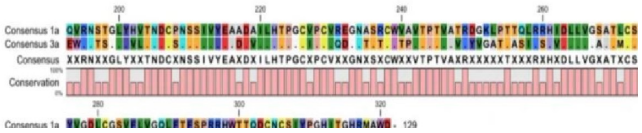

Figure 11: The multiple sequence alignment links the HCV E1 genotype 3a and 1a segregated from different parts of the world to universal consensus sequence. The cryptic alignment symbols are represented by (X), whereas the identical leftovers are shown as (.) [49]

Up to 11 N-Linked glycosylation sites are present on envelope protein E2, which participates in viral entry by interacting with human CD81's extracellular loop, the scavenger receptor class B type 1 /SRB-1), the high viscosity lipoprotein (HDL) binding molecule and the mannose binding proteins DC-SIGN and L-SIGN. Although both glycoproteins are crucial for viral entry, designing vaccines or inhibitory compounds against them is difficult due to their hyper variability. in order to identify conderved peptides in HCV that could serve as valuable targets in the creation of new inhibitory composites and lower the risk of HCV in Pakistan, the study was done to perform a sequence analysis of E1 and E2 among genotypes 3a and 1a. A technique that was grounded in consensus was employed to create efficient peptides. For the HCV E1 (Figure 11) and E2 (Figure 12) proteins, a global consensus sequence was created utilizing the multiple alignment point of the CLC workbench. Recaptured from the NCBI protein database, the HCV E1 and E2 sequences of genotypes 3a and 1a were then subjected to conservation analysis utilizing the multiple sequence alignment feature of the CLC workbench. small peptides of 8 to 25 amino acids were created from the largely conserved residues of E1, and using the same criteria, small peptides of the largely conserved portions of E2 were also created. Given that the 1a and 3a genotypes share these peptides, they may be beneficial for creating peptide-based vaccinations and inhibitory composites.

Figure 12: The multiple sequence alignment links the HCV E1 genotype 3a and 1a segregated from different parts of the world to the universal consensus sequence. The cryptic alignment symbols are represented by (X), whereas the identical leftovers are shown as (.) [49]

Both proteins' phylogenetic trees revealed groupings built on the basis of evolutionary relatedness. It can be concluded that the envelope proteins of genotype 3a, which are geographically isolated, are connected to genotype 1a from many nations and have a common evolutionary ancestor. Additionally, it is implied that a common strain exists between genotypes 1a and 3a. Thus, it can be said that HCV E1 and E2 are related to genotype 1a and 3a in other nations in terms of evolution. Figure 13 displays the evolutionary tree of the E1 protein, while Figure 14 displays the evolutionary tree of the HCV E2 protein.

From the NCBI protein database, 150 HCV E1 and E2 sequences belonging to genotypes 3a and 1a were retrieved. The multiple sequence analysis criterion of the CLC workbench was used to create consensus sequences of E1 and E2 proteins for each genotype. These consensus sequences were then utilized to create E1 and E2 global consensus sequences. Except for Baluchistan, where genotype 1a is the most recent genotype, genotype 3a is reported as the most recent genotype in Pakistan. The goal of this work was to find possibly conserved peptides in the HCV E1 and E2 hypervariable proteins. Largely conserved and variable regions were identified through conservation analysis, and from the variable regions, peptides were created that could potentially be used as targets for the creation of new inhibitory composites that are effective against both the 3a and 1a genotypes, protecting the Pakistani population from the threat

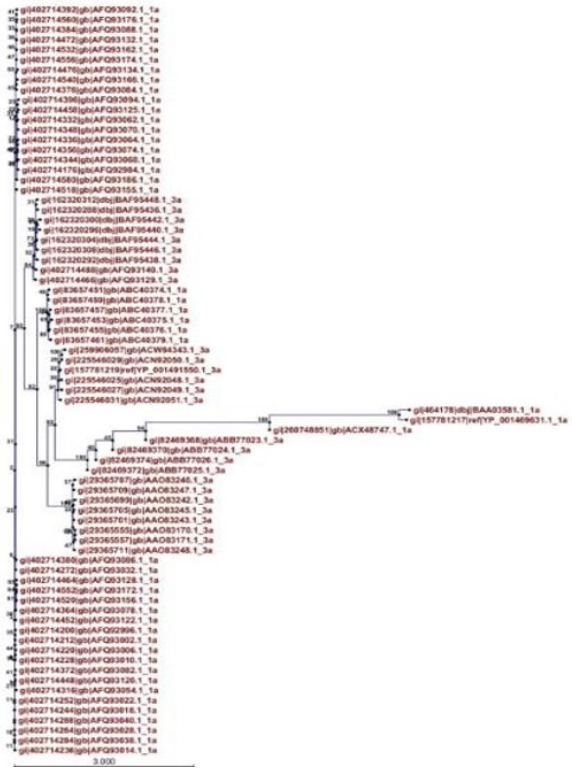

Figure 13: Phylogenetic Tree displaying Evolutionary links between HCV E1 proteins from genotypes 3a and 1a from various geographical locations [49]

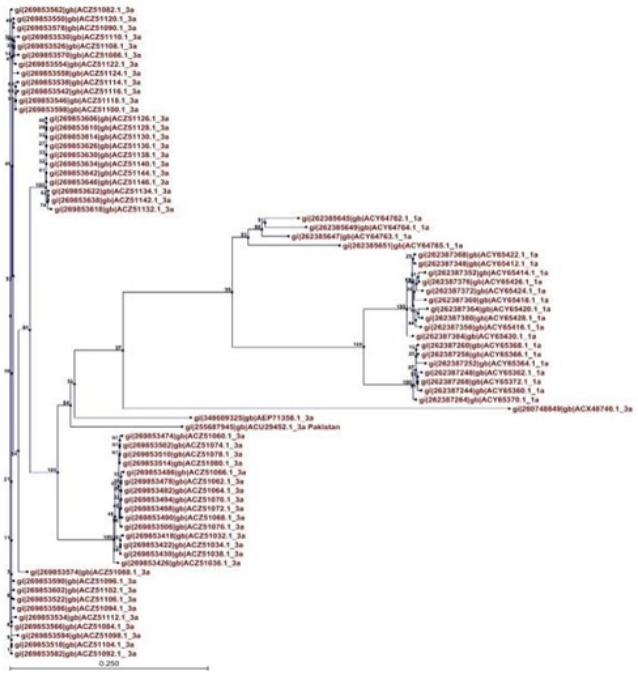

Figure 14: Phylogenetic Tree displaying Evolutionary links between HCV E1 proteins of genotypes 3a and 1a from various geographical Locations [49]

of HCV infection. The evolutionary relationships between various genetic variations or strains of the virus are shown visually in a phylogenetic tree of the HCV envelope protein E2. The evolutionary tree for the Hepatitis C virus´ E2 envelope protein is displayed below

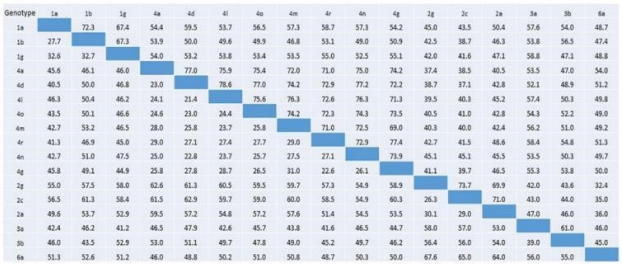

Figure 15: Analysis of HCV E1 protein's percentage nucleotide identity and divergence using the pairwise distance maximum likelihood technique via MEGA 7 [50]

A phylogenetic study was completed in 2019 using 278 sequences at random, representing all genotypes, historical periods, and isolation countries. Distance-based neighbor- joining was used to build the phylogenetic tree with MEGA® V.7.0 software (1,000 replication bootstrap values) [50]. To create a phylogenetic tree, reference genotype sequences were obtained from the https://hcv.lanl.gov database. In order to analyze E1 nucleotide mutations and amino acid changes, all obtained sequences were further pairwise aligned with genotype-specific reference sequences using the MAFFT program. The identification of nucleotide mutations and relative residue analysis of all the sequences were performed using the BioEdit® V.5.0.6(17) program. A different and genotype- specific distribution pattern was shown by the phylogenetic study of the HCV E1 gene. All E1 sequences came together in various clades representing their various genotypes. Between genotypes 1a and 1b, 2c and 2g, and 4a, 4d, and 4o, there is a higher level of nucleotide identity in the E1 residue, according to the pairwise analysis of inheritable distances (Figure 15).

Except for one sequence that was connected to both the 5a and 6a genotypes that belonged to Algeria and Iran separately, the majority of the retrieved sequences belonged to genotypes 1, 2, 3, and 4. A total of 19 genotypes (subtypes) were built in the phylogenetic tree. The phylogenetic analysis revealed the E1 protein's evolutionary dynamics for the dispersed distribution of different HCV genotypes and subtypes in the MENA area. In this respect, the genotype 4a was the most prevalent, followed by 3a and 2c. The highest genotype and subtype diversity was found in South Arabia (G- 1(1a, 1b, 1g), G- 2(2a, 2c), G- 3(3a), and G- 4(4a, 4d, 4n, 4o, 4r, 4s)). Egypt (G- 1(1b, 1g) and G- 4(4a, 4l, 4n, 4m, 4u), Iran (G- 1(1b) and G- 3.

References

[1] N. A. Z. M. Amin, T. N. A. M. Jusoh, A. A. Irekeola, R. H. Shueb, Hepatitis c: A review on current and emerging genotyping assays., Malaysian Journal of Medicine & Health Sciences 19 (5).

[2] L. Puchades Renau, M. Berenguer, Introduction to hepatitis c virus infection: Overview and history of hepatitis c virus therapies, Hemodialysis International 22 (2018) S8–S21.

[3] B. Maasoumy, H. Wedemeyer, Natural history of acute and chronic hepatitis c, Best practice & research Clinical gastroenterology 26 (4) (2012) 401–412.

[4] S. K. Sarin, M. Kumar, Natural history of hcv infection, Hepatology international 6 (2012) 684–695.

[5] H. Basit, I. Tyagi, J. Koirala, Hepatitis, c. statpearls, in: Hepatitis CStatPearls, StatPearls Publishing Treasure Island (FL), 2023.

[6] N. Salari, M. Kazeminia, N. Hemati, M. Ammari-Allahyari, M. Mohammadi, S. Shohaimi, Global prevalence of hepatitis c in general population: A systematic review and meta-analysis, Travel medicine and infectious disease 46 (2022) 102255.

[7] J. Yang, J.-L. Qi, X.-X. Wang, X.-H. Li, R. Jin, B.-Y. Liu, H.-X. Liu, H.-Y. Rao, The burden of hepatitis c virus in the world, china, india, and the united states from 1990 to 2019, Frontiers in Public Health 11 (2023) 1041201.

[8] U. Saleem, N. Aslam, R. Siddique, S. Iqbal, M. Manan, Hepatitis c virus: Its prevalence, risk factors and genotype distribution in pakistan, European Journal of Inflammation 20 (2022) 1721727X221144391.

[9] R. Z. A. Khan, R. S. A. Khan, U. A. Khan, L. Alam, S. R. A. Naqvi, S. Z. A. Naqvi, Chronic hcv infection-comparison of awareness regarding mode of transmission in educated and uneducated patients presenting in gastroenterology/medical clinics in various hospitals of sindh province, Pakistan Armed Forces Medical Journal 72 (5) (2022) 1739.

[10] J.-H. Kao, D.-S. Chen, Transmission of hepatitis c virus in asia: past and present perspectives, Journal of gastroenterology and hepatology 15 (2000) E91–E96.

[11] M. J. Alter, Hcv routes of transmission: what goes around comes around, in: Seminars in liver disease, Vol. 31, © Thieme Medical Publishers, 2011, pp. 340–346.

[12] T. Pietschmann, R. J. Brown, Hepatitis c virus, Trends in microbiology 27 (4) (2019) 379–380.

[13] H. Wan, R. L. Adams, B. D. Lindenbach, A. M. Pyle, The in vivo and in vitro architecture of the hepatitis c virus rna genome uncovers functional rna secondary and tertiary structures, Journal of Virology 96 (8) (2022) e01946–21.

[14] M. T. Deniz, S. Akhan, Hepatitis c virus structure and diagnostic methods, in: Hepatitis C-Recent Advances, IntechOpen, 2023.

[15] G. Dupré, R. Volmer, Influence of viral genome properties on polymerase fidelity, Trends in Genetics 39 (1) (2023) 9–14.

[16] S. Faiz, M. Irfan, S. Farooq, I. A. Khan, H. Iqbal, A.-t. Wahab, M. Shakeel, P. Gong, T. Iftner, M. I. Choudhary, Study of drug resistance-associated genetic mutations, and phylo-genetic analysis of hcv in the province of sindh, pakistan, Scientific Reports 13 (1) (2023) 12213.

[17] J. J. Germer, J. N. Mandrekar, J. L. Bendel, P. S. Mitchell, J. D. Yao, Hepatitis c virus genotypes in clinical specimens tested at a national reference testing laboratory in the united states, Journal of clinical microbiology 49 (8) (2011) 3040–3043.

[18] D. Zarębska-Michaluk, Genotype 3-hepatitis c virusÂ´ last line of defense, World Journal of Gastroenterology 27 (11) (2021) 1006.

[19] G. Schnell, R. Tripathi, P. Krishnan, J. Beyer, T. Reisch, M. Irvin, T. Dekhtyar, C. Setze, L. Rodrigues-Jr, K. Alves, et al., Resistance characterization of hepatitis c virus genotype 2 from japanese patients treated with ombitasvir and paritaprevir/ritonavir, Journal of Medical Virology 90 (1) (2018) 109–119.

[20] K. Al Naamani, S. Al Sinani, M. Deschênes, Epidemiology and treatment of hepatitis c genotypes 5 and 6, Canadian Journal of Gastroenterology and Hepatology 27 (1) (2013) e8–e12.

[21] E. Gupta, J. Samal, A. Pandey, G. Singh, H. A. Gupta, R. Agarwal, M. K. Sharma, Treatment response and drug resistance profiling of genotype 6 of hepatitis c virus in hcv/hiv co-infected patients: a pilot study from india, Viruses 14 (5) (2022) 944.

[22] P. Guntipalli, R. Pakala, S. Kumari Gara, F. Ahmed, A. Bhatnagar, M. Endaya Coronel, A. Razzack, A. Solimando, A. Thompson, K. Andrews, et al., Worldwide prevalence, genotype distribution and management of hepatitis c, Acta Gastroenterol Belg 84 (4) (2021) 637–656.

[23] A. Ahmad, M. R. Khan, R. Naz, H. Akbar, Prevalence of hcv in tehsil babozi district swat, khyber-pakhtunkhwa, pakistan, International Journal of Scientific and Engineering Research 12 (3) (2021) 789–797.

[24] P. Falson, B. Bartosch, K. Alsaleh, B. A. Tews, A. Loquet, Y. Ciczora, L. Riva, C. Montigny, C. Montpellier, G. Duverlie, et al., Hepatitis c virus envelope glycoprotein e1 forms trimers at the surface of the virion, Journal of virology 89 (20) (2015) 10333–10346.

[25] D. Sepulveda-Crespo, S. Resino, I. Martinez, Hepatitis c virus vaccine design: focus on the humoral immune response, Journal of Biomedical Science 27 (2020) 1–12.

[26] Y. Tong, X. Chi, W. Yang, J. Zhong, Functional analysis of hepatitis c virus (hcv) envelope protein e1 using a trans-complementation system reveals a dual role of a putative fusion peptide of e1 in both hcv entry and morphogenesis, Journal of Virology 91 (7) (2017) 10–1128.

[27] Y. Tong, D. Lavillette, Q. Li, J. Zhong, Role of hepatitis c virus envelope glycoprotein e1 in virus entry and assembly, Frontiers in immunology 9 (2018) 1411.

[28] G. Vieyres, J. Dubuisson, T. Pietschmann, Incorporation of hepatitis c virus e1 and e2 glycoproteins: the keystones on a peculiar virion, Viruses 6 (3) (2014) 1149–1187.

[29] N. Echeverría, G. Moratorio, J. Cristina, P. Moreno, Hepatitis c virus genetic variability and evolution, World journal of hepatology 7 (6) (2015) 831.

[30] M. R. Oliver, K. Toon, C. B. Lewis, S. Devlin, R. J. Gifford, J. Grove, Evidence of a novel viral membrane fusion mechanism shared by the hepaci, pegi and pestiviruses, bioRxiv (2022) 2022–10.

[31] F. Stoll-Keller, H. Barth, S. Fafi-Kremer, M. B. Zeisel, T. F. Baumert, Development of hepatitis c virus vaccines: challenges and progress, Expert Review of Vaccines 8 (3) (2009) 333–345.

[32] A. Nayak, N. Pattabiraman, N. Fadra, R. Goldman, S. L. Kosakovsky Pond, R. Mazumder, Structure–function analysis of hepatitis c virus envelope glycoproteins e1 and e2, Journal of Biomolecular Structure and Dynamics 33 (8) (2015) 1682–1694.

[33] A. G. Khan, J. Whidby, M. T. Miller, H. Scarborough, A. V. Zatorski, A. Cygan, A. A. Price, S. A. Yost, C. D. Bohannon, J. Jacob, et al., Structure of the core ectodomain of the hepatitis c virus envelope glycoprotein 2, Nature 509 (7500) (2014) 381–384.

[34] P. Neddermann, L. Tomei, C. Steinkühler, P. Gallinari, A. Tramontano, R. De Francesco, The nonstructural proteins of the hepatitis c virus: structure and functions., Biological chemistry 378 (6) (1997) 469–476.

[35] A. Sabahi, S. L. Uprichard, W. C. Wimley, S. Dash, R. F. Garry, Unexpected structural features of the hepatitis c virus envelope protein 2 ectodomain, Journal of virology 88 (18) (2014) 10280–10288.

[36] G. Sautto, A. W. Tarr, N. Mancini, M. Clementi, Structural and antigenic definition of hepatitis c virus e2 glycoprotein epitopes targeted by monoclonal antibodies, Journal of Immunology Research 2013 (1) (2013) 450963.

[37] N. Kato, Y. Ootsuyama, T. Tanaka, M. Nakagawa, T. Nakazawa, K. Muraiso, S. Ohkoshi, M. Hijikata, K. Shimotohno, Marked sequence diversity in the putative envelope proteins of hepatitis c viruses, Virus Research 22 (2) (1992) 107–123.

[38] D. Smith, Evolution of the hypervariable region of hepatitis c virus, Journal of Viral Hepatitis 6 (1999) 41–46.

[39] A. J. Weiner, H. M. Geysen, C. Christopherson, J. E. Hall, T. J. Mason, G. Saracco, F. Bonino, K. Crawford, C. D. Marion, K. A. Crawford, Evidence for immune selection of hepatitis c virus (hcv) putative envelope glycoprotein variants: potential role in chronic hcv infections., Proceedings of the National Academy of Sciences 89 (8) (1992) 3468–3472.

[40] Y. Alhammad, J. Gu, I. Boo, D. Harrison, K. McCaffrey, P. T. Vietheer, S. Edwards, C. Quinn, F. Coulibaly, P. Poumbourios, et al., Monoclonal antibodies directed toward the hepatitis c virus glycoprotein e2 detect antigenic differences modulated by the n-terminal hypervariable region 1 (hvr1), hvr2, and intergenotypic variable region, Journal of virology 89 (24) (2015) 12245–12261.

[41] H. Freedman, M. R. Logan, J. L. M. Law, M. Houghton, Structure and function of the hepatitis c virus envelope glycoproteins e1 and e2: antiviral and vaccine targets, ACS Infectious Diseases 2 (11) (2016) 749–762.

[42] W. P. Hofmann, C. Sarrazin, B. Kronenberger, B. Schönberger, K. Bruch, S. Zeuzem, Mutations within the cd81-binding sites and hypervariable region 2 of the envelope 2 protein: Correlation with treatment response in hepatitis c virus–infected patients, The Journal of infectious diseases 187 (6) (2003) 982–987.

[43] A. Albecka, R. Montserret, T. Krey, A. W. Tarr, E. Diesis, J. K. Ball, V. Descamps, G. Duverlie, F. Rey, F. Penin, et al., Identification of new

functional regions in hepatitis c virus envelope glycoprotein e2, Journal of virology 85 (4) (2011) 1777–1792.

[44] A. Torrents de la Peña, K. Sliepen, L. Eshun-Wilson, M. L. Newby, J. D. Allen, I. Zon, S. Koekkoek, A. Chumbe, M. Crispin, J. Schinkel, et al., Structure of the hepatitis c virus e1e2 glycoprotein complex, Science 378 (6617) (2022) 263–269.

[45] L. J. Ströh, T. Krey, Hcv glycoprotein structure and implications for b-cell vaccine development, International Journal of Molecular Sciences 21 (18) (2020) 6781.

[46] A. G. Khan, M. T. Miller, J. Marcotrigiano, Hcv glycoprotein structures: what to expect from the unexpected, Current opinion in virology 12 (2015) 53–58.

[47] M. C. Metcalf, B. M. Janus, R. Yin, R. Wang, J. D. Guest, E. Pozharski, M. Law, R. A. Mariuzza, E. A. Toth, B. G. Pierce, et al., Structure of engineered hepatitis c virus e1e2 ectodomain in complex with neutralizing antibodies, Nature Communications 14 (1) (2023) 3980.

[48] L. J. Ströh, T. Krey, Structural insights into hepatitis c virus neutralization, Current Opinion in Virology 60 (2023) 101316.

[49] S. Idrees, U. A. Ashfaq, N. Idrees, Development of global consensus sequence of hcv glycoproteins involved in viral entry, Theoretical Biology and Medical Modelling 10 (2013) 1–7.

[50] M. U. Sohail, Y. Hadi Muhamad, A. T. Asma A, Comparative phylogenetic and residue analysis of hepatitis c virus e1 protein from the middle east and north africa region.

Available online at www.rpnsci.com

ISSN (P): 3006-8452, ISSN (O): 3006-8460

Research Prospects in Natural Sciences, Vol. 2, Issue 2, (2024) 13–16

Research Article

Antioxidant activity of methanolic extracts of sweet lime (*Citrus lemitta*) peel, pulp, and seed by 2, 2-diphenyl-1-picryl-hydrazyl free radical

Zafar Iqbal[a,*], Aisha Naz[b], Amna Shaheen[b], Mian Habib ur Rehman Mahmood[b], Muhammad Khalid Saeed[c]

[a]*Applied Chemistry Research Centre, PCSIR Labs. Complex, Lahore 54600, Pakistan*
[b]*Department of Chemistry, University of Education, Township, Lahore 54770, Pakistan*
[c]*Food & Biotechnology Research Centre, PCSIR Labs. Complex, Lahore 54600, Pakistan*

Abstract

Sweet lime (*Citrus lemitta*) fruits were collected from a local market in Lahore Pakistan, their peels, pulp, and seed were separated manually and dried under shade for 20 days. After drying, their extracts were prepared separately by immersing each component in methanol at a ratio of 1:5 (w/v) for 14 days at ambient conditions. The antioxidant activity of each extract was evaluated by using 2,2-diphenyl-1-picryl-hydrazyl radical. Butylated hydroxyl toluene was used as a standard, and the percentage inhibition was determined for each extract. The results indicate that peel methanolic extract with concentrations of 25μL, 50μL, 75μL and 100μL has DPPH inhibition of 70%, 74.3%, 79.1%, and 81.2% respectively. Pulp methanolic extract with concentrations of 25μL, 50μL, 75μL and 100μL have DPPH inhibition 65.3%, 69.7%, 74.1%, and 77.1% respectively. Seed methanolic extract with the same concentration has DPPH inhibition 46.2%, 49.7%, 54.6%, and 58.9% respectively. The antioxidant activity of all the extracts was concentration-dependent.

Keywords:
Sweet Lime, Peel, Pulp, Seed, Methanolic Extract, Antioxidant activity, DPPH.

1. Introduction

Citrus Lemitta belongs to the family Rutaceae, it has approximately 158 genera and 1900 species, which includes citrus [1]. In Punjab, Pakistan it is known as "Mitha". It is sweet, flavorful, full of juice and vitamin C. About 4% of the world´s citrus production comes from Pakistan, and its export contribution is merely 0.8% [2]. Citrus trees are grown almost everywhere in Pakistan, however, Punjab contributes the most to production, which is almost 70% [3]. Around the world, citrus is grown in more than 80 different countries and the most prominent producers are Pakistan, India, Egypt, and Palestine [4]. Ten species of the genus Citrus are found in Pakistan. Among them is *Citrus limetta* var. Mitha is sometimes known as sweet lime. It is a well-known native citrus fruit that is enjoyed in several regions of the subcontinent for its delicious culinary qualities in addition to its cooling and medicinal properties. Sweet lime juice has therapeutic benefit in treating fever, malaria, and jaundice according to the traditional indigenous medical system [5]. The fruit sweet lime is full in bioactive components like minerals, vitamin C, and phenolic compounds [6]. Ten species of the genus Citrus are found in Pakistan. One piece of sweet lime has total weight 159g, out of which seed, peel and pulp has 3.3g, 25g and 130.5g weight respectively. The endocarp and pericarp are the two distinct sections that make up a citrus fruit. The pericarp is made up of peel that has a lot of aromatic oil glands, which give the fruit its distinct aroma and gloss. After juice extraction, citrus fruits contribute significant amounts of non-edible residues up to 80%, which includes peel, pulp, and seeds and these are referred as "agri-wastes" [7]. After processing, the peel makes up between 30 and 40 percent of the entire citrus fruit mass that is discarded as trash. This peel can be used to make value-added goods and to fortify food items to improve the nutritional profile. If this trash is not used, it may create an unpleasant odor, contaminate the soil, serve as an insect colony, and seriously harm the ecosystem. Only the pulp of the citrus fruit is used in the juice industry, and a sizable portion of the peel and seed are thrown away as waste. Even though citrus peel has a high nutraceuti-

*Corresponding Author:
zafarmayo2000@yahoo.com (Zafar Iqbal)

cal value, it can be used as a functional ingredient in the form of powder for the food, pharmaceutical, and cosmetic industries to promote health. This is important because it promotes health and helps us make better use of the peel waste while also protecting our environment from pollution caused by waste citrus peel [8]. Methanolic extract of Sweet lime Peel, Pulp and Seed were prepared to examine their antioxidant activity. Supplying the body with antioxidants from external sources is crucial, as they help to lower the risk of heart disease and boost immunity. Oxidative stress can arise from free radicals, which include reactive oxygen species and reactive nitrogen species produced within our bodies. Maintaining a balance between free radicals and antioxidants is crucial for proper physiological function. Free radicals can negatively impact lipids, proteins, and DNA, contributing to various human diseases. Therefore, utilizing external sources of antioxidants can help mitigate oxidative stress. It's worth noting that synthetic antioxidants like butylated hydroxytoluene and butylated hydroxyanisole have recently been identified as posing potential risks to human health [9] The peel, comprising nearly half of the fruit mass, harbors the highest levels of flavonoids in Citrus fruits. Numerous studies have highlighted the presence of antioxidants in the juice and consumable sections of oranges, originating from various sources and varieties. Regarding the peel, extracts from this particular fruit component have demonstrated a notable overall radical antioxidative capacity [10]. The free radical 2,2-diphenyl-1-picrylhydrazyl (DPPH) method were employed to assess the antioxidant properties of both crude extracts and isolated compounds. In general, seeds exhibited superior antioxidant activity compared to peels. The composition analysis of all examined samples using HPLC revealed that methanol extracts were abundant in flavones and glycosylated flavanones, while hydrolyzed extracts primarily contained phenolic acids and flavonols. However, no discernible correlation was observed between antioxidant activity and the phenolic composition of the extracts [11]. *Citrus limetta* is a juicy fruit and after its juice extraction, other materials like peels, pulp and seeds are being discarded as waste. The significance of this study is to prepare methanolic extract to examine its antioxidant activity.

2. Materials and Methods

2.1. Collection of Material

Sweet lime were collected from local vegetable market of Lahore, Punjab Pakistan. Their Peel, Pulp and Seed separated, kept under shade at ambient conditions and dried for 20 days.

2.2. Chemicals

Purchased following analytical grade chemicals from the market of Lahore, Punjab Pakistan for methanolic extraction and antioxidant activity of Peel and Pulp and Seed. Methanol, DPPH (2,2-diphenyl-1-picrylhydrazyl)

2.3. Methanolic Extraction

Methanolic extraction of Peel, Pulp and Seed were prepared.

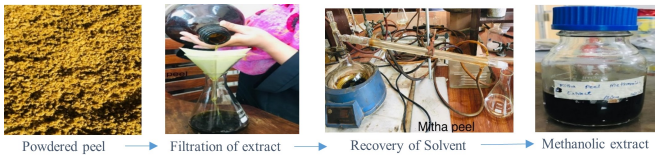

2.3.1. Methanolic extraction of Peel

Peels were dried and grounded into powder using a grinder machine to enhance the surface area and were passed through the 500mm mesh. 100g of peel powder were taken in a 1000ml sealed container and added 500 ml methanol in it. The mixture was macerate for 16 days with frequent shaking. After that filtered the mixture using filter paper to separate the solid residue from the liquid extract. The liquid extract was concentrated to eliminate the solvent through a distillation method. The resulting concentrates were transferred to airtight sample bottle and stored at room temperature.

2.3.2. Methanolic extraction of Pulp

Grounded the dried pulp into powder form using a grinder machine. From this powder added 100g in to 500ml of methanol and put in a 1000ml airtight container. After maceration of 16 days filtered this mixture using filter paper to remove the solid residue from the liquid extract. Concentrated the liquid extract to eliminate the solvent through a distillation method. The resulting concentrates was transferred to airtight sample bottle and stored at room temperature.

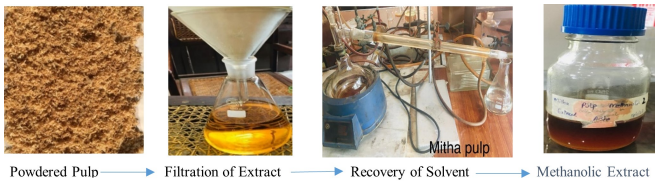

2.3.3. Methanolic extraction of Seed

Seeds were dried, grounded into powder form to increase the surface area. 100g of this powder was taken, added into 500ml methanol and kept in a sealed jar. Macerated for 16 days, filtered the mixture using filter paper to separate the solid residue from the liquid extract. Concentrated the liquid extract through distillation to remove the solvent. Transferred the resulting concentrate to an airtight sample bottle and stored it at room temperature.

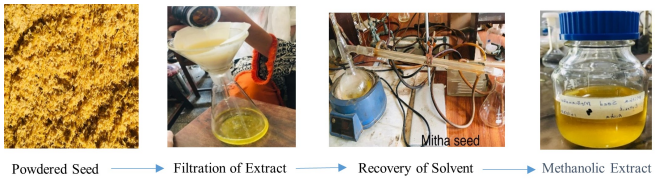

2.4. Antioxidant Activity of Methanolic Extracts

Antioxidant activity of methanolic extracts from sweet lime seed, peel and pulp was assessed using the 2,2-diphenyl-1-picrylhydrazyl (DPPH) radical method, as outlined by [12]. The

methanolic extracts of sweet lime seed, peel, and pulp, at concentrations 25μL, 50μL, 75μL and 100μL, were combined with 3 ml of methanol containing DPPH solution. After 30-minutes incubation at room temperature, the absorbance of the resulting solution and the blank (containing only DPPH) was measured at a wavelength of 517 nm using a UV-Vis spectrophotometer. The percentage inhibition of these extracts is determined by the following equation

$$\%\ \text{Inhibation (DPPH)} = \frac{Absorbance\ of\ blank\ solution - Absorbance\ of\ sample}{Absorbance\ of\ blank\ solution} \times 100$$

3. Results

3.1. Antioxidant Activity of Sweet Lime Peel

Peel methanolic extract has higher antioxidant activity due to the presence of phenolic content. Literature showed that the juices obtained from *citrus lemitta* peeled fuits had higher phenolic content such as limonene, linalool, β-myrcene and β-citronellol [6].Peel methanolic extract with concentration 25μL, 50μL, 75μL and 100μL have 70%, 74.3%, 79.1% and 81.2% DPPH inhibition respectively These results have been shown in fig.(1)

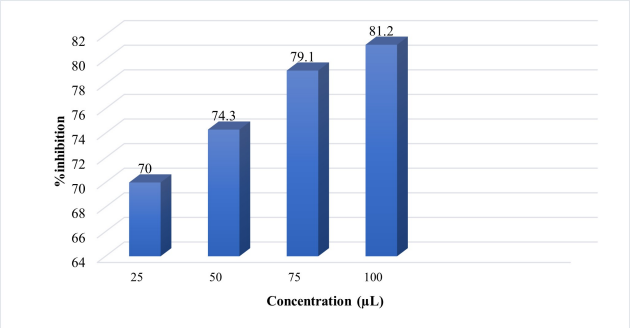

Figure 1: Antioxidant activity of Sweet Lime Peel Methanolic Extract

3.2. Antioxidant Activity of Sweet Lime Pulp

Only the pulp of the citrus fruit is used in the juice industry, and a sizable portion of the peel and seed are thrown away as waste. After juice extraction pulp residue is also thrown away. Methanolic extract of this pulp was prepared which showed DPPH inhibion of 65.3%, 69.7%, 74.1% and 77.1% at concentration of 25μL, 50μL, 75μL and 100μL respectively as shown in fig.(2)

3.3. Antioxidant Activity of Sweet Lime Seed

Citrus seed had limonoids, along with phenolic compounds like phenolic acids, flavonoids, tocopherols, and carotenoids. The positive impact of these components on human health was recognized. Citrus seed extracts had prominent phenolic acids such as caffeic, p-coumaric, and ferulic acids [13]. Al-Anbari et. al. [14] showed that seed ethanolic extract had higher quantities of phenolic content free radic al scavenging activity, total flavonoides, chelating Fe^{+2} ions, and the ability to scavenge

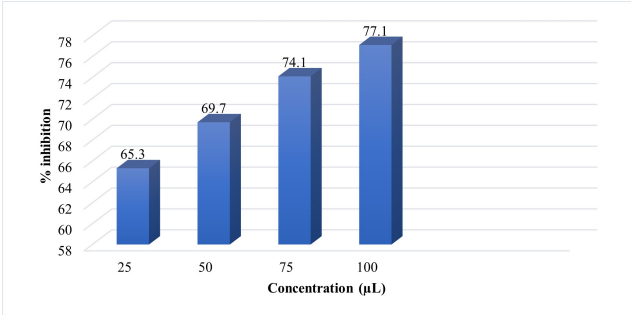

Figure 2: Antioxidant activity of Sweet lime Pulp Methanolic Extract

hydrogen peroxide. The results indicate that Seed methanolic extract with concentration 25μL, 50μL, 75μL and 100μL have DPPH inhibition 46.2%, 49.7%, 54.6% and 58.9% respectively, as shown in fig.(3)

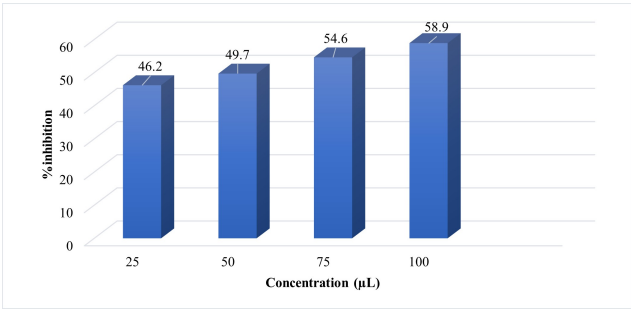

Figure 3: Antioxidant activity of Sweet lime Seed Methanolic Extract

4. Discussion

The existing literature highlights over 170 antioxidants were found in Citrus fruits, encompassing vitamins, phenolic compounds, mineral elements, terpenoids, and pectin [15]. Literature showed that the juices obtained from *citrus lemitta* peeled and unpeeled fuits had phenolic content of 109 mg/L and 88.9 mg/L respectively, while the antioxidant activities were 118 Mm Trolox/L and 93.2 Mm Trolox/L [6]. Li et. al. [16] revealed that grapefruit peels exhibit a higher total phenolic content than the peels of mandarin, yeb Ben lemon, orange, and meyer lemon. Especially the peels of lemon, orange, and grapefruit are rich in phenolic compounds and vitamin C, exhibiting a high rate of antioxidant activity. The correlation between total phenolic content and antioxidant activity, especially in the peels, was more pronounced compared to the alternative factor. A positive correlation between antioxidant activity and total phenolic content suggests that phenolics may play a significant role in the antioxidant capacities of these fruit residues. The analysis by Sir Elkhatim et. al.[17] demonstrated that peels contained elevated levels of phenolic compounds, flavonoids, vitamin C, and antioxidant activity compared to their inner discarded components including pulp and seeds. Among the peels,

grapefruit exhibited the highest total phenolic content, measuring 77.3 mg of gallic acid equivalent/g of peels, followed by lemon with 49.8 mg and orange with 35.6 mg. Vitamin C content of 113.3, 330.4, and 58.59 mg/100 g were identified in grapefruit, orange, and lemon peels respectively. However, the antioxidant activity of orange pulp and seeds was greater than that of grapefruit and lemon. According to Abeysinghe et. al.[18] and Goulas et. al.[19] the peel of citrus fruits is noted to possess a higher concentration of bioactive compounds as compared to the pulp. The ability of phenolic compounds to exhibit antioxidant activity arises from the existence of phenolic hydroxyl groups, which readily contribute a hydrogen atom or an electron to free radicals. Additionally, an extended conjugated aromatic system facilitates the delocalization of an unpaired Electron [20]. Results showed Sweet lime peel methanolic extract had higher activity of 81.2% while literature reported 755.78μM Trolex Equivalent (TE) [21]. Methanolic extract of sweet lime pulp showed antioxidant activity of 77.1% having concentration of 100μL while results reported that the orange pulp had 99.14mmol Trolox/g [22]. He also reported that sweet lime peel had higher antioxidant activity than pulp due to the presence of higher phenolic content [22]. While the sweet lime seed methanolic extract had antioxidant activity of 58.9% with concentration of 100μL at 517nm wavelength while literature showed that ethanolic seed extract of sour oranges had 60.4% which is nearly equivalent to our results [14]. As compared to other citrus fruits the antioxidant activity of *Citrus lemitta* can vary depending on fruit culture, area and growth conditions. Extraction method also effect both phenolic content and antioxidant activity of Sweet lime Peel, Seed, and Pulp.

References

[1] D. J. Mabberley, et al., Mabberley's Plant-book: a portable dictionary of plants, their classifications and uses., no. Ed. 3, Cambridge university press, 2008.

[2] A. Tahir, Forecasting citrus exports in pakistan, Pakistan Journal of Agricultural Research 27 (1).

[3] A. Nawaz, W. Ahmed, M. Jiskani, High density planting-an approach to increase citrus yields (2007).

[4] K. Chang, The evaluation of citrus demand and supply, Proceeding of International Society Citric. Italy 3 (1992) 1153–1155.

[5] M. M. Cowan, Plant products as antimicrobial agents, Clinical microbiology reviews 12 (4) (1999) 564–582.

[6] D. Topi, Volatile and chemical compositions of freshly squeezed sweet lime (citrus limetta) juices, The Journal of Raw Materials to Processed Foods 1 (1) (2020) 22–27.

[7] A. Zayed, M. T. Badawy, M. A. Farag, Valorization and extraction optimization of citrus seeds for food and functional food applications, Food Chemistry 355 (2021) 129609.

[8] M. Iftikhar, S. Wahab, N. ul Haq, S. N. Malik, S. Amber, N. U. Taran, S. U. Rehman, Utilization of citrus plant waste (peel) for the development of food product, Pure and Applied Biology (PAB) 8 (3) (2019) 1991–1998.

[9] Z. Iqbal, H. K. Mehmood, M. Hussain, M. Mehmood, M. N. Choudhry, Antioxidant activity of essential oil from the leaves and stems of murraya koenigii, World Journal of Pharmaceutical Research 6 (7) (2017) 267–273.

[10] N. J. Miller, C. A. Rice-Evans, The relative contributions of ascorbic acid and phenolic antioxidants to the total antioxidant activity of orange and apple fruit juices and blackcurrant drink, Food Chemistry 60 (3) (1997) 331–337.

[11] A. Bocco, M.-E. Cuvelier, H. Richard, C. Berset, Antioxidant activity and phenolic composition of citrus peel and seed extracts, Journal of agricultural and food chemistry 46 (6) (1998) 2123–2129.

[12] A. L. Dawidowicz, D. Wianowska, M. Olszowy, On practical problems in estimation of antioxidant activity of compounds by dpph method (problems in estimation of antioxidant activity), Food chemistry 131 (3) (2012) 1037–1043.

[13] B. Falcinelli, F. Famiani, A. Paoletti, S. DÂ´Egidio, F. Stagnari, A. Galieni, P. Benincasa, Phenolic compounds and antioxidant activity of sprouts from seeds of citrus species, Agriculture 10 (2) (2020) 33.

[14] A. K. H. Al-Anbari, M. A. Hasan, Antioxidant activity in some citrus leaves and seeds ethanolic extracts, AABES London UK (2015) 93–7.

[15] Z. Zou, W. Xi, Y. Hu, C. Nie, Z. Zhou, Antioxidant activity of citrus fruits, Food chemistry 196 (2016) 885–896.

[16] B. Li, B. Smith, M. M. Hossain, Extraction of phenolics from citrus peels: I. solvent extraction method, Separation and Purification Technology 48 (2) (2006) 182–188.

[17] K. A. Sir Elkhatim, R. A. Elagib, A. B. Hassan, Content of phenolic compounds and vitamin c and antioxidant activity in wasted parts of sudanese citrus fruits, Food science & nutrition 6 (5) (2018) 1214–1219.

[18] D. Abeysinghe, X. Li, C. Sun, W. Zhang, C. Zhou, K. Chen, Bioactive compounds and antioxidant capacities in different edible tissues of citrus fruit of four species, Food chemistry 104 (4) (2007) 1338–1344.

[19] V. Goulas, G. A. Manganaris, Exploring the phytochemical content and the antioxidant potential of citrus fruits grown in cyprus, Food chemistry 131 (1) (2012) 39–47.

[20] J. Dai, R. J. Mumper, Plant phenolics: extraction, analysis and their antioxidant and anticancer properties, Molecules 15 (10) (2010) 7313–7352.

[21] O. K. Buyukkurt, G. Guclu, H. Kelebek, S. Selli, Characterization of phenolic compounds in sweet lime (citrus limetta) peel and freshly squeezed juices by lc-dad-esi-ms/ms and their antioxidant activity, Journal of Food Measurement and Characterization 13 (2019) 3242–3249.

[22] H. R. de Moraes Barros, T. A. P. de Castro Ferreira, M. I. Genovese, Antioxidant capacity and mineral content of pulp and peel from commercial cultivars of citrus from brazil, Food chemistry 134 (4) (2012) 1892–1898.

Available online at www.rpnsci.com

ISSN (P): 3006-8452, ISSN (O): 3006-8460

Research Prospects in Natural Sciences, Vol. 2, Issue 2, (2024) 17–20

Research Article

Antioxidant potential of biogenically synthesized silver nanoparticles using *Prunus armenica* fruit extract

Farhad[a], Anam Sajid[b,*], Arfaa Sajid[c], Qaisar Manzoor[c], Saira Ishaq[d]

[a]*School of Chemistry, University of The Punjab, Lahore, Quaid e Azam Campus, 54580, Lahore, Pakistan*
[b]*Natural Sciences and Humanities Department, University of Engineering and Technology Lahore, New campus, Pakistan*
[c]*Department of Chemistry, The University of Lahore, Lahore, Pakistan*
[d]*Department of Chemistry, Government College University, Lahore, Pakistan*

Abstract

Nanotechnology has been an interdisciplinary science that combines physics, chemistry, engineering, biology. Silver nanoparticles (AgNPs) work as the next generation, anti-economic agent, having good pharmaceutical potential. In this work synthesis of silver nanoparticle was carried out using Prunus armeniaca fruit extract, which was used as a reducing and stabilizing agents. Spectral analysis of AgNPs were done by UV-Visible spectroscopy and Fourier Transform Infrared Spectroscopy (FTIR). While, for morphological analysis Scanning Electron Microscopic (SEM) analysis, Energy Dispersive spectroscopy analysis (EDS) and X-Ray Diffraction (XRD) techniques were used. The antioxidant potential of AgNPs was checked by DPPH assay. It revealed maximum 84.76% inhibition of DPPH radical.

Keywords:
Nanotechnology, Green synthesis, Silver nanoparticles, *Prunus armeniaca*

1. Introduction

Nanotechnology has transformed numerous scientific disciplines by introducing innovative solutions in medicine, environmental science, and materials engineering. Among the diverse types of nanoparticles, silver nanoparticles (AgNPs) have gained significant attention due to their wide ranging biological activities, including anti-inflammatory, antimicrobial, and anticancer properties [1, 2]. Beyond these well established functions, the antioxidant potential of AgNPs has emerged as promising area of investigation, particularly for addressing disorders associated with oxidative stress.

Oxidative stress results from an imbalance between reactive oxygen species (ROS) and antioxidant defenses, contributing to a range of pathological conditions such as cardiovascular diseases, neurodegenerative disorders, and cancer [3]. Elevated ROS levels can damage cells by inducing lipid peroxidation, protein degradation, and DNA mutations. Although both natural and synthetic antioxidants have been widely studied, challenges related to their bioavailability and stability have highlighted the need for alternative approaches. Due to their high surface area-to-volume ratio and customizable physicochemical properties, AgNPs have demonstrated considerable potential as effective free radical scavengers [4].

The antioxidant activity of AgNPs is strongly influenced by factors such as particle size, shape, surface charge, and synthesis method. Green synthesis techniques, which employ plant extracts or microbial agents, provide eco-friendly alternatives while also enhancing the biocompatibility and functionality of AgNPs [5]. These biologically synthesized nanoparticles exhibit significant reducing power and free radical scavenging capabilities, largely due to the bioactive compounds present on their surfaces.

Prunus armeniaca, commonly known as an apricot, is a fruit-bearing tree belonging to the Rosaceae family and is renowned for its nutritional and medicinal properties. The apricot is widely cultivated across temperate regions and has been traditionally used in various cultural systems of medicine because of its health-promoting effects. Its applications range from treating respiratory ailments and digestive disorders to supporting skin health and managing chronic diseases [6]. The therapeutic potential of P. armeniaca lies in its rich composition of bioactive compounds, including phenolic acids, carotenoids, flavonoids, vitamins (notably vitamins A and C), and amygdalins. These com-

*Corresponding Author:
anam.sajid@uet.edu.pk (Anam Sajid)

pounds possess antioxidant, anti-inflammatory, antimicrobial, hepatoprotective, and anticancer properties [7].

This study investigates the antioxidant properties of silver nanoparticles synthesized using Prunus armenica. This research aims to support the development of AgNP-based therapeutic solutions to combat oxidative stress and its related health challenges.

2. Materials and Methods

2.1. Preparation of apricot extract

P. armenica fruit was purchased from the local market. It was washed to remove dust particles. Further washing was done with distilled water to clean it properly and kept it for drying. Then fruit seeds were removed, and fruit was cut into small pieces. 50 g of apricot fruit was boiled in 500 ml of distilled water for 30 minutes at 60 °C in a water bath. *P armenica* fruit extract was cooled, filtered by using a sieve and kept in refrigerator for further use.

2.2. Green synthesis of silver nanoparticles

80 ml of 3 mM solution of silver nitrate was added in 10 ml *P. armenica* fruit extract. The mixture was stirred for 2 hours at 60 °C. The color of solution was changed from pale yellow to dark brown indicating the formation of silver nanoparticle. The mixture was centrifuged for 30 mints at speeds of 8000 revolutions per minute (rpm). After that silver nanoparticles were collected and stored.

Figure 1: Schematic diagram for Green synthesis of AgNPs

2.3. Characterization of silver nanoparticles

Spectral studies of AgNPs were done by UV-Vis and FTIR spectroscopy. Repeated time scans were performed between 200-800 nm with UV-Visible spectrophotometer (Lambda 25, Perkin Elmer, USA) to determine the synthesis of AgNPs. The FTIR analysis of AgNPs was performed using potassium bromide (KBr) pellet method in a ratio of 1:100 and the spectrum was recorded on Shimadzu FTIR spectrophotometer in transmission mode. Morphological evaluation of silver nanoparticles was carried out using SEM and XRD techniques. The images of AgNPs were obtained on a Field Emission Scanning-Electron Microscope (FE-SEM, JSM7500F) at an accelerating voltage of 10 keV.

The crystalline structure of the biosynthesized AgNPs was checked through powder x-ray diffraction method by using a Rigaku Multiflex X-ray powder diffractometer involving CuKα radiation (0.154nm) operating between 10°and 80°at the scanning rate of 2°per min. The crystalline size was then calculated by using Scherrer´s equation.

2.4. Antioxidant activity of silver nanoparticles

The antioxidant activity of synthesized nanoparticles was determined by DPPH (2, 2-diphenyl-1-picrylhydrazyl) assay by following procedure [8]. Different concentrations of AgNPs 25, 50, 75, 100 μg/mL were used. 1 mL of nanoparticles solution was added to 3 mL of 0.1 mM DPPH solution. This mixture was kept for 30 minutes at incubation in dark. The absorbance was noted at 517 nm. Ascorbic acid was used as positive standard. Reaction was run in triplicate.

3. Results and Discussion

3.1. Characterization of AgNPs

3.1.1. Spectral examination of AgNPs

Silver nanoparticles were characterized by UV-Visible spectroscopy. Figure 2 represented the UV-Visible spectra of synthesized AgNPs which was plotted as a function of time. It clearly revealed the strong resonance centred at 430 nm with increased intensity in 90 minutes. The color change from yellow to brown started in 30 mint and remain persistent after 90 minutes representing the completion of reduction of silver ions. Similar color changes have been noticed in the reported literature [9]. The flavonoids present in the plant extract are responsible for reduction of silver ions in silver nitrate solution [10]. It is evident from literature that AgNP showed UV-Visible absorbance in the range of 428-430 nm [11, 12].

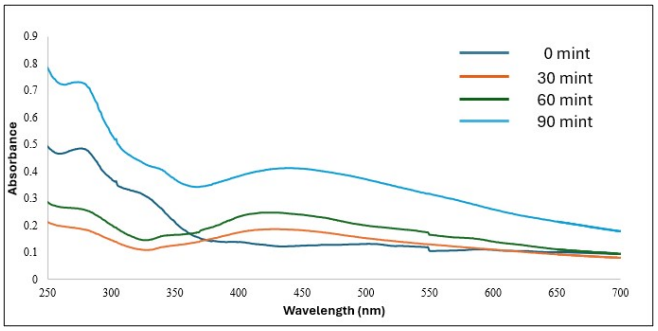

Figure 2: UV-Visible Spectra of AgNPs synthesized by *P. armenica* fruit extract

FTIR analysis was used to identify the various functional group involved in reduction of Ag to AgNPs. FTIR spectrum shown in figure 3. The peak at 3326 cm^{-1} assigned to OH vibration of phenolic content in fruit extract. Apricot fruit is a rich source of phenolics including catechin, epicatechin, chromogenic and neochlorogenic acids [13]. The peak at 1718 cm^{-1} assigned to C=O stretching vibrations of carbonylic moiety in the fruit extract. The band at 1341 cm^{-1} was associated with

the C-H bending vibrations of methyl group. The C-O stretching peak appeared at 1010 cm^{-1}. While the peak at 830 cm^{-1} attributed to C-H bending vibrations.

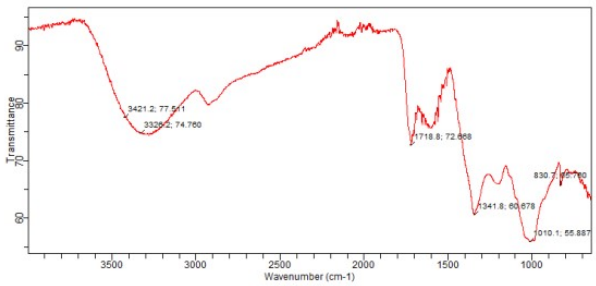

Figure 3: FTIR Analysis of silver nanoparticle

3.2. Morphological examination of AgNPs

3.2.1. Scanning Electron Microscopy

The morphology of silver nanoparticles was determined by SEM images which are shown in Figure 4. SEM images taken at various resolutions illustrated that the silver nanoparticles are spherical in shape highlighted by green circles in figure 4. SEM images also confirmed the formation of individual AgNPs along with some aggregates of AgNPs.

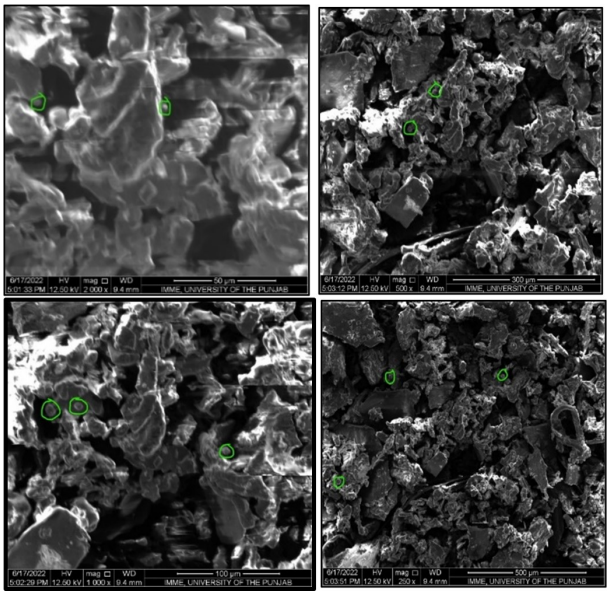

Figure 4: Scanning Electron Microscopy images of silver nanoparticle at various resolutions

3.2.2. Energy Dispersive Spectroscopy analysis

The formation of silver nanoparticles by biological reduction was further confirmed by EDS spectra. In EDS analysis various areas had been focused and corresponding peaks are shown in figure 5. EDS spectra clearly indicate the presence of Ag in tested material. The presence of oxygen may be due to the adsorption of extracellular organic moieties on the surface of nanoparticles. The presence of Mg and K was due to the X-ray emission of different minerals present in apricot fruit extract [14].

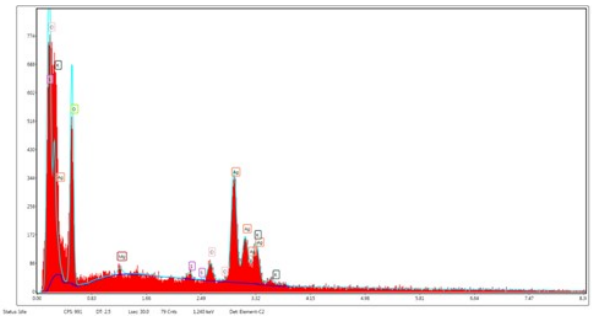

Figure 5: Energy Dispersive Spectrum of silver nanoparticle

3.2.3. X-Ray Diffraction Analysis

The crystalline structure of the bio-synthesized AgNPs was confirmed through powder X-ray diffraction (XRD) analysis as shown in Figure 6. The presence of silver nanocrystals was indicated by distinct Bragg reflection peaks observed at 20 values of 38.82°, 44.06°, 64.19°, and 77.21°, corresponding to the (111), (200), (220), and (311) crystallographic planes, respectively. These findings suggest that the synthesized AgNPs exhibit a face-centered cubic (fcc) structure. The same XRD pattern has been reported by Garibo et al., 2020 [15].

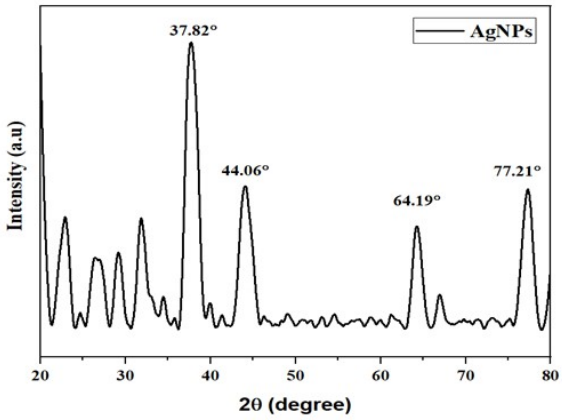

Figure 6: XRD pattern of biogenic Ag nanoparticles crystal structure of silver

3.2.4. XRD pattern of biogenic Ag nanoparticles. crystal structure of silver

Silver nanoparticles prepared by using fruit extract of P. armenecia inhibited DPPH radical, results are shown in figure 7. The percentage inhibition was increased by increasing the concentration of AgNPs. The maximum inhibition of DPPH radical was observed 84.76% at a AgNPs concentration of 100 μg/mL which is comparable to ascorbic acid used as positive control. Similar results for antioxidant activity of biogenically synthesized AgNPs have been reported in literature [16, 17].

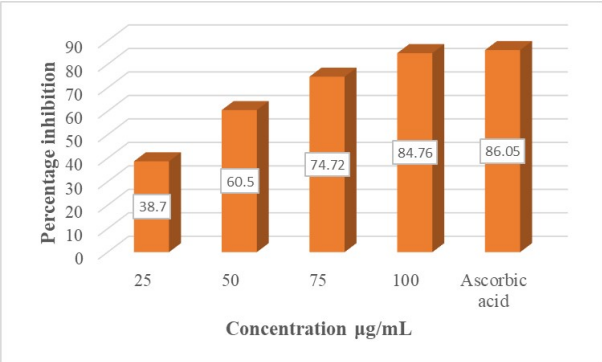

Figure 7: Percentage inhibition of DPPH radical by biogenically synthesizedAgNPs

4. Conclusion

Green synthesis of silver nanoparticles was carried out using Prunus armenica fruit extract. These nanoparticles were characterized by UV-Visible and FTIR spectroscopy. For morphological insight of AgNPs SEM and XRD were used. Results of all these analyses confirmed the successful formation of AgNPs. These nanoparticles were examined for their antioxidant potential, and they inhibited the DPPH radical upto 84.76% which is comparable to standard ascorbic acid. It is concluded that biogenically synthesized AgNPs hava good therapeutic potential and can be further studied against various illnesses.

References

[1] S. Ahmed, M. Ahmad, B. L. Swami, S. Ikram, et al., Green synthesis of silver nanoparticles using azadirachta indica aqueous leaf extract, Journal of radiation research and applied sciences 9 (1) (2016) 1–7.

[2] M. Rai, A. Yadav, A. Gade, Silver nanoparticles as a new generation of antimicrobials, Biotechnology advances 27 (1) (2009) 76–83.

[3] M. Valko, D. Leibfritz, J. Moncol, M. T. Cronin, M. Mazur, J. Telser, Free radicals and antioxidants in normal physiological functions and human disease, The international journal of biochemistry & cell biology 39 (1) (2007) 44–84.

[4] S. Gurunathan, J. Raman, S. N. A. Malek, P. A. John, S. Vikineswary, Green synthesis of silver nanoparticles using ganoderma neo-japonicum imazeki: a potential cytotoxic agent against breast cancer cells, International journal of nanomedicine (2013) 4399–4413.

[5] S. Priyadarshini, S. Sulava, R. Bhol, S. Jena, Green synthesis of silver nanoparticles using azadirachta indica and ocimum sanctum leaf extract, Current Science 117 (8) (2019) 1300–1307.

[6] D. Kitic, B. Miladinovic, M. Randjelovic, A. Szopa, J. Sharifi-Rad, D. Calina, V. Seidel, Anticancer potential and other pharmacological properties of prunus armeniaca l.: an updated overview, Plants 11 (14) (2022) 1885.

[7] G. Kamel, N. E. Awad, A. A. Shokry, et al., Phytochemical screening, acute toxicity, analgesic and anti-inflammatory effects of apricot seeds ethanolic extracts, Journal of Applied Veterinary Sciences 3 (1) (2018) 26–33.

[8] U. Younas, S. Iqbal, A. Saleem, R. Rahman, A. Nazir, F. Hassan, A. Sajid, Z. Saeed, M. Iqbal, N. Ahmad, Evaluation of biological activity and pharmacological attributes of pariploca aphylla: potential source of functional food and nutraceuticals, Rev. Roum. Chim. 68 (7–8) (2023) 391–400.

[9] A. Sajid, Q. Manzoor, A. Sajid, M. Imran, S. Khalid, Z. Arshad, A. Saleem, F. Aslam, Characterization and antibacterial properties of eriobotrya japonica extract loaded silver-nanoparticles, Current Bioactive Compounds 17 (7) (2021) 58–63.

[10] J. Huang, G. Zhan, B. Zheng, D. Sun, F. Lu, Y. Lin, H. Chen, Z. Zheng, Y. Zheng, Q. Li, Biogenic silver nanoparticles by cacumen platycladi extract: synthesis, formation mechanism, and antibacterial activity, Industrial & Engineering Chemistry Research 50 (15) (2011) 9095–9106.

[11] A. Sajid, R. Javed, Q. Manzoor, A. Sajid, A. Saleem, F. Imtiaz, S. Ahmed, H. Nadeem, Development of ag–ceo2 bimetallic nanocomposite for visible-light-induced photocatalytic degradation of eriochrome black t, Chemistry Africa 7 (4) (2024) 2103–2110.

[12] P. Logeswari, S. Silambarasan, J. Abraham, Synthesis of silver nanoparticles using plants extract and analysis of their antimicrobial property, Journal of Saudi Chemical Society 19 (3) (2015) 311–317.

[13] T. Kan, M. Gundogdu, S. Ercisli, F. Muradoglu, F. Celik, M. K. Gecer, O. Kodad, M. Zia-Ul-Haq, Phenolic compounds and vitamins in wild and cultivated apricot (prunus armeniaca l.) fruits grown in irrigated and dry farming conditions, Biological Research 47 (2014) 1–6.

[14] O. Alajil, V. R. Sagar, C. Kaur, S. G. Rudra, R. Sharma, R. Kaushik, M. K. Verma, M. Tomar, M. Kumar, M. Mekhemar, Nutritional and phytochemical traits of apricots (prunus armeniaca l.) for application in nutraceutical and health industry, Foods 10 (6) (2021) 1344.

[15] D. Garibo, H. A. Borbón-Nuñez, J. N. D. de León, E. García Mendoza, I. Estrada, Y. Toledano-Magaña, H. Tiznado, M. Ovalle-Marroquin, A. G. Soto-Ramos, A. Blanco, et al., Green synthesis of silver nanoparticles using lysiloma acapulcensis exhibit high-antimicrobial activity, Scientific reports 10 (1) (2020) 12805.

[16] S. N. Kharat, V. D. Mendhulkar, Synthesis, characterization and studies on antioxidant activity of silver nanoparticles using elephantopus scaber leaf extract, Materials Science and Engineering: C 62 (2016) 719–724.

[17] S. Bhakya, S. Muthukrishnan, M. Sukumaran, M. Muthukumar, Biogenic synthesis of silver nanoparticles and their antioxidant and antibacterial activity, Applied Nanoscience 6 (2016) 755–766.

Available online at www.rpnsci.com

ISSN (P): 3006-8452, ISSN (O): 3006-8460

Research Prospects in Natural Sciences Vol. 2, Issue 2, (2024) 21–25

Research Article

TE and TM surface waves at the interface of a left-handed metamaterial

Burhan Zamir[a,*], Saeed Ilyas[b], Babar Shahzad[b]

[a]*Department of Physics, Govt. M. A. O. Graduate College, Lahore 54000, Pakistan*
[b]*Department of Physics, Division of Science & Technology, University of Education, Lahore 54700, Pakistan.*

Abstract

In this paper, we present an analytical treatment for the electromagnetic surface waves propagating at the interface of a linear right-handed material and a linear left-handed material. In this connection, we use Maxwell equations to find the electric and magnetic field components corresponding to the transverse electric (TE) and transverse magnetic (TM) wave polarizations. Electromagnetic boundary conditions are then employed on the field components at the interface to find the dispersion relations for both TE and TM waves. These dispersion relations are reduced to the case of TE and TM surface waves propagation along an interface between two different right-handed media. The dispersion relations are then analyzed numerically by plotting them for the propagation frequency and the wave vector for both wave modes. Some features of waves propagating at these interfaces are found to be useful in microwave device applications.

Keywords:
TE surface waves, TM surface waves, left-handed material.

1. Introduction

The fabrication and investigation of novel materials developed modern applied physics. Among these materials, the best known examples are the metamaterials, photonic band-gap materials and birefringent media, due to their unique electromagnetic properties [1–8]. The class of metamaterials with simultaneously negative permittivity and permeability in a specific range of frequency show some peculiar electrodynamic properties [4, 9, 10] and therefore used to improve the working of optical and microwave devices etc. These metamaterials are known as left-handed materials (LHMs) [11]because the wave vector makes a left-handed set of vectors with electric and magnetic fields. In 1968, Vesselago [12] first time gave the idea of left-handed materials and suggested some unusual phenomena including negative refraction. Later, due to the work of Pendry et al. [13–15], Smith et al. [9] and Shelby et al. [4], these materials were physically realized [9] by fabricating artificially engineered structures showing the simultaneously negative permittivity and permeability in a certain range of frequency. Since then, various authors reported a lot of research work in connection with these left-handed materials for their practical applications to optical and microwave devices (e.g., [5, 16, 17])

In the recent years, a considerable work has been done to study the surface and guided waves on interfaces of various modern materials [18–20] and employed on waveguide and sandwich structures for their development and applications to the communication devices etc. For example, Shadrivov et al. [11] study the surface at the interface of nonlinear left-handed media. In this analysis, they discussed the possibility of tuning the group velocity of the wave with the help of nonlinearity of the LHM. Maimistov and Lyashko [18] theoretically studied the surface waves propagating along an interface between an isotropic dielectric and a topological insulator. They derived the dispersion relation for both TE and TM modes and found that the two modes are in superimposed form. El-Khozondar et al.[21] investigated the guiding electromagnetic waves along ferroelectric / metamaterial interface. This work is related to the derivation and numerical solution of the dispersion relation, which shows the dependence of dispersion characteristics on nonlinearity of ferroelectric material.

In the present work, we theoretically analysed both TE and TM surface waves propagating along an interface between a linear right-handed material (RHM) and a linear left-handed material (LHM). A planar symmetry is used in the theoretical model to describe TE and TM wave modes. The dispersion relation for RHM/LHM interface is derived and is reduced to RHM/RHM interface. This work may find its importance for the design and

*Corresponding Author:
burhanzamir1@gmail.com (Burhan Zamir)

development of different communication devices, such as integrated circuits, transmission lines and antennas systems etc., operating at microwave frequencies.

2. Theoretical analysis

Surface electromagnetic waves at the interface between a right handed and a left-handed medium, as shown in Figure 1 had been studied

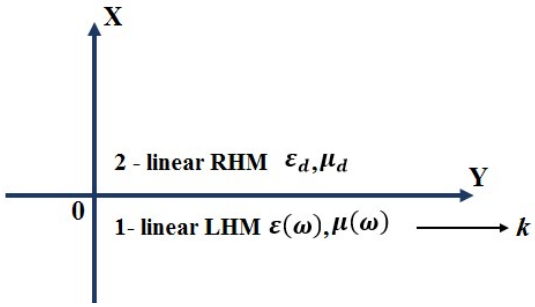

Figure 1: Surface waves at RHM/LHM interface

An electromagnetic surface wave is propagating in y- direction with propagation constant k and frequency ω at conventional linear RHM (at $x < 0$) and a LHM (at $x > 0$). Both the media are infinitely extended in yz-plane. The RHM is specified by the constant (positive) relative permittivity and permeability ε_d and μ_d, whereas, for LHM, the negative values of relative permittivity and permeability are given by the frequency dependent functions given by

$$\varepsilon(\omega) = 1 - \frac{\omega_p^2}{\omega^2} \tag{1}$$

$$\mu(\omega) = 1 - \frac{F\omega^2}{\omega^2 - \omega_r^2} \tag{2}$$

where ω_p is the plasma frequency, ω_r is the resonance frequency and F is the filling factor [9]. Here, without loss of generality, the damping terms are not considered [19]. The field profiles for transvers electric (TE) and transverse magnetic (TM) waves have the following forms:

$$\text{TE Waves}: \begin{cases} E = [0, 0, E_z(\omega, x)]\, e^{i(\omega t - ky)} \\ H = \left[H_x(\omega, x), H_y(\omega, x), 0\right] e^{i(\omega t - ky)} \end{cases} \tag{3}$$

$$\text{TM Waves}: \begin{cases} E = \left[E_x(\omega, x), E_y(\omega, x), 0\right] e^{i(\omega t - ky)} \\ H = [0, 0, H_z(\omega, x)]\, e^{i(\omega t - ky)} \end{cases} \tag{4}$$

2.1. Field components for left-handed material at $x < 0$

To obtain the electromagnetic wave equation for the left-handed material, we first take the Maxwell field equations for the LHM as

$$\nabla \times H = i\omega\varepsilon_\circ \varepsilon(\omega) E \tag{5}$$

$$\nabla \times E = -i\omega\mu_\circ \mu(\omega) H \tag{6}$$

For the case of TE surface waves, equations 3 - 6 have been used to obtain the following wave equation for E_{Z_1}:

$$\frac{d^2 E_{z_1}}{dx^2} - k^2 E_{z_1} + k_\circ^2 \mu(\omega)\varepsilon(\omega) E_{z_1} = 0 \tag{7}$$

where $K_\circ^2 = \frac{\omega^2}{c^2}$. The solution of the above wave equation is given by

$$E_{z_1} = a_1 e^{k_1 x} + a_2 e^{-k_1 x} \tag{8}$$

Here $K_1 = \left[K^2 - K_\circ^2 \mu(\omega)\varepsilon(\omega)\right]^{\frac{1}{2}}$. a_1, a_2 are arbitrary constants and can be evaluated from the boundary conditions. For LHM (region 1), the following TE field components $E_{Z_1}(\omega, x)$, $H_{x_1}(\omega, x)$, and $H_{y_1}(\omega, x)$ are obtained from (5), (6) and (8), and here we assume that the field penetration length in LHM is much shorter than its dimensions:

$$E_{z_1}(\omega, x) = a_1 e^{k_1 x} \tag{9}$$

$$H_{x_1}(\omega, x) = \frac{k}{\omega\mu_\circ \mu(\omega)} (a_1 e^{k_1 x}) \tag{10}$$

$$H_{y_1}(\omega, x) = \frac{-ik_1}{\omega\mu_\circ \mu(\omega)} (a_1 e^{k_1 x}) \tag{11}$$

A similar mathematical treatment can be performed to calculate the following field components corresponding to TM waves:

$$H_{z_1}(\omega, x) = a_1' e^{k_1 x} \tag{12}$$

$$E_{x_1}(\omega, x) = \frac{-k}{\omega\varepsilon_\circ \varepsilon(\omega)} (a_1' e^{k_1 x}) \tag{13}$$

$$E_{y_1}(\omega, x) = \frac{ik_1}{\omega\varepsilon_\circ \varepsilon(\omega)} (a_1' e^{k_1 x}) \tag{14}$$

2.2. Field components for linear dielectric at $x > 0$

To obtain the electromagnetic wave equation for the linear dielectric medium, we first take the Maxwell field equations for the LHM as

$$\nabla \times H = i\omega\varepsilon_\circ \varepsilon_d E \tag{15}$$

$$\nabla \times E = -i\omega\mu_\circ \mu_d H \tag{16}$$

For the case of TE surface waves, equations (15) and (16) have been used to obtain the following wave equation for E_{z_2} :

$$\frac{d^2 E_{z_2}}{dx^2} - k^2 E_{z_2} + k_\circ^2 \varepsilon_d \mu_d E_{z_2} = 0 \tag{17}$$

The solution of the above wave equation is given by

$$E_{z_2} = c_1 e^{k_2 x} + c_2 e^{-k_2 x} \tag{18}$$

Here $K_2 = \left[K^2 - K_\circ^2 \varepsilon_d \mu_d\right]^{\frac{1}{2}}$. c_1 and c_2 are arbitrary constants and can be evaluated from the boundary conditions. For linear dielectric medium (region 2), the following TE field components $E_{z_2}(\omega, x)$, $H_{x_2}(\omega, x)$ and $H_{y_2}(\omega, x)$ are obtained from (15), (16) and (18), and here we assume that the field penetration length in linear dielectric is much shorter than its dimensions:

$$E_{Z_2}(\omega, x) = c_2 e^{-k_2 x} \tag{19}$$

$$H_{x_2}(\omega, x) = \frac{k}{\omega \mu_\circ \mu_d}(c_2 e^{-k_2 x}) \tag{20}$$

$$H_{y_2}(\omega, x) = \frac{ik_2}{\omega \mu_\circ \mu_d}(c_2 e^{-k_2 x}) \tag{21}$$

A similar mathematical treatment can be performed to calculate the following field components corresponding to TM waves:

$$H_{Z_2}(\omega, x) = c_2' e^{-k_2 x} \tag{22}$$

$$E_{x_2}(\omega, x) = \frac{-k}{\omega \varepsilon_\circ \varepsilon_d}(c_2' e^{-k_2 x}) \tag{23}$$

$$E_{y_2}(\omega, x) = \frac{-ik_2}{\omega \varepsilon_\circ \varepsilon_d}(c_2' e^{-k_2 x}) \tag{24}$$

2.3. The dispersion relation

To find the dispersion relation for the TE and TM waves, we employ the following boundary conditions for the continuity of the tangential field components at $x = 0$:

$$\text{TM Waves} : \begin{cases} E_{z_1}|_{x=0} & = E_{z_2}|_{x=0} \\ H_{y_1}|_{x=0} & = H_{y_2}|_{x=0} \end{cases} \tag{25}$$

$$\text{TM Waves} : \begin{cases} H_{z_1}|_{x=0} & = H_{z_2}|_{x=0} \\ E_{y_1}|_{x=0} & = E_{y_2}|_{x=0} \end{cases} \tag{26}$$

Using the values of $E_{z_1}(\omega, x)$, $E_{z_2}(\omega, x)$, $H_{y_1}(\omega, x)$ and $H_{y_2}(\omega, x)$ from equations (9), (11), (19) and (21) in equation (25) to obtain the following dispersion relation of the TE surface waves at the interface between a linear dielectric and a left-handed medium:

$$\frac{k_1}{\mu(\omega)} + \frac{k_2}{\mu_d} = 0 \tag{27}$$

Similarly, using the values of $H_{z_1}(\omega, x)$, $H_{z_2}(\omega, x)$, $E_{y_1}(\omega, x)$ and $E_{y_2}(\omega, x)$ from equations (12), (14), (22) and (24) to equation (26) to obtain the following dispersion relation of the TM surface waves at the interface between a linear dielectric and a left-handed medium:

$$\frac{k_1}{\varepsilon(\omega)} + \frac{k_2}{\varepsilon_d} = 0 \tag{28}$$

3. The Numerical Results

In this section, we numerically study the dispersion relations (27) and (28) for the TE and TM polarized waves propagating along LHM/RHM interface. In this connection, we show the dependence of wave vector k on the propagation frequency, within the existence frequency band of LHM. For a comparison of dispersion characteristics, we reduce the dispersion relation for LHM/RHM interface to RHM/RHM interface.

To plot the dispersion relations (27) and (28), we first express them as explicit functions of ω and k. For this purpose, we substitute the values of k_1 and k_2, defined in equations (8) and (18), to equations (27) and (28), to obtain the following forms of the dispersion relations:

$$\text{TE Waves} : k = \pm \frac{\omega}{c} \left\{ \frac{\mu(\omega)\mu_d(\varepsilon_d \mu(\omega) - \varepsilon(\omega)\mu_d)}{(\mu^2(\omega) - \mu_d^2)} \right\}^{\frac{1}{2}} \tag{29}$$

$$\text{TM Waves} : k = \pm \frac{\omega}{c} \left\{ \frac{\varepsilon(\omega)\varepsilon_d(\mu_d \varepsilon(\omega) - \mu(\omega)\varepsilon_d)}{(\varepsilon^2(\omega) - \varepsilon_d^2)} \right\}^{\frac{1}{2}} \tag{30}$$

Equations (29) and (30) represent dispersion relations for TE and TM polarized waves for the RHM/LHM interface. We can obtain the following dispersion relations for the RHM/RHM interface [22] by substituting $\varepsilon(\omega)$, $\mu(\omega)$, ε_d and μ_d by ε_{d_1}, μ_{d_1}, ε_{d_2} and μ_{d_2} respectively in equations (29) and (30):

$$\text{TE Waves} : k = \pm \frac{\omega}{c} \left\{ \frac{\mu_{d_1}\mu_{d_2}(\varepsilon_{d_2}\mu_{d_1} - \varepsilon_{d_1}\mu_{d_2})}{(\mu_{d_1}^2 - \mu_{d_2}^2)} \right\}^{\frac{1}{2}} \tag{31}$$

$$\text{TM Waves} : k = \pm \frac{\omega}{c} \left\{ \frac{\varepsilon_{d_1}\varepsilon_{d_2}(\mu_{d_2}\varepsilon_{d_1} - \mu_{d_1}\varepsilon_{d_2})}{(\varepsilon_{d_1}^2 - \varepsilon_{d_2}^2)} \right\}^{\frac{1}{2}} \tag{32}$$

3.1. Numerical Analysis of RHM/RHM interface

To obtain the dispersion characteristics of TE and TM surface waves propagating at the interface between two different dielectric media with positive signs of permittivity and permeability, we plot equation (31) and (32) for the numerical values ε_{d_1}=3, μ_{d_1}=4, ε_d=1, μ_{d_2}=2 respectively. Figure 2 shows a plot of propagation frequency ω versus the wave vector k for the surface waves propagating along RHM/RHM interface, for both TE and TM waves and for the whole microwave range of frequency. The graph shows that for both TE and TM polarizations, the surface waves propagate for the whole range of frequency but the propagation is prominent above a frequency $\omega \sim 10^{11} Hz$. It can be seen that the values of wave vector k are very small below $\omega \sim 10^{11} Hz$. This fact is useful for the microwave propagation devices e.g., filters, sensors, frequency selectors etc. Further, the dispersion curves for TE and TM wave modes have a difference in their order of magnitudes as they are separating each other continuously after $\omega \sim 10^{11} Hz$. Therefore, the wave polarizations TE and TM can tune the device according to the desired pair of values for frequency and wave vector.

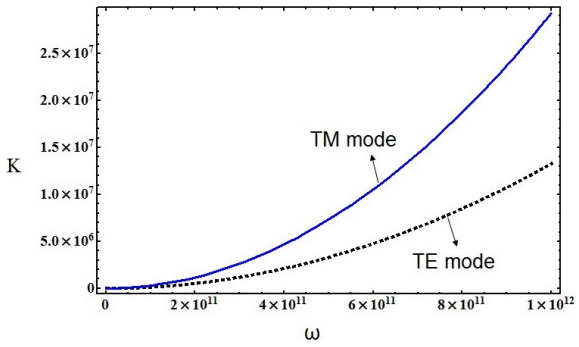

Figure 2: A plot of propagation frequency ω and wave vector k for surface wave propagating at RHM/RHM interface

3.2. Numerical Analysis of RHM/LHM Structure

To plot the dispersion characteristics for a LHM/RHM structure, we first find the frequency range in which the permittivity and permeability have simultaneously negative signs. For this purpose, we plot relative permittivity $\varepsilon(\omega)$ and relative permeability $\mu(\omega)$ given in Equations (1) and (2) against the propagation frequency as shown in Figure 3. For this plot, the numerical values of the physical parameters are given as: F = 0.56, $\omega_r = 4 \times 10^9 Hz$ and $\omega_p = 10 \times 10^9 Hz$ [9, 11]. Figure 3 shows that the frequency range for the simultaneously negative values of permittivity and permeability is from $4GHz$ to $6GHz$.

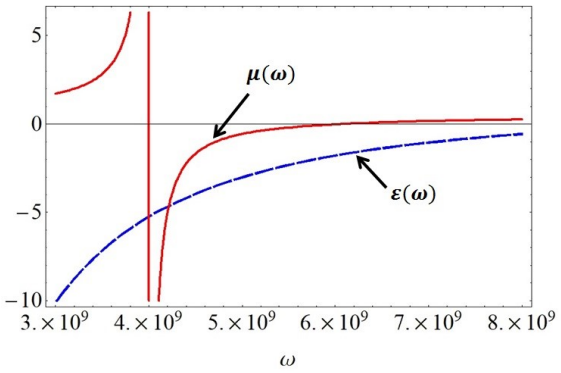

Figure 3: A plot between permittivity and permeability (i.e. $\varepsilon(\omega)$ and $\mu(\omega)$) of left-handed material against the operating frequency ω

To obtain the dispersion characteristics of TE and TM surface waves propagating at the interface between a right handed dielectric medium and a left-handed medium., we use the following numerical values in Equations (29) and (30): F = 0.56, $\omega_r = 4 \times 10^9 Hz$, $\omega_p = 10 \times 10^9 Hz$, $\varepsilon_d = 2$ and $\mu_d = 4$ [9, 11].

Figure 4 shows a plot of surface wave propagation frequency ω versus the wave vector k for the RHM/LHM interface, for both TE and TM waves and for the frequency band of a left-handed medium extended from 4 GHz to 6 GHz. The dispersion curve for TM wave polarization shows continues decrease at higher frequencies which is in contrast to the dispersion characteristics of the TM polarization of RHM/RHM structure. Due to this fact, our proposed RHM/LHM interface can be used to design a low pass filter for the TM surface waves within the existence band of the left-handed material i.e. 4 to 6 GHz.

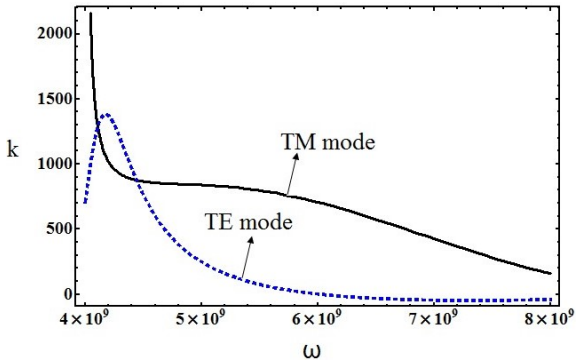

Figure 4: A plot between permittivity and permeability (i.e. $\varepsilon(\omega)$ and $\mu(\omega)$) of left-handed material against the operating frequency ω

Further, it can also be seen that at lower side of the frequency band of the LHM, the dispersion curve for the TE wave polarization shows a sudden increase in amplitude and then it decreases continuously at higher values of frequency. This fact suggests that the proposed interface can be used for the designing of a band pass filter for the TE surface waves (for only lower frequency side of the LHM frequency band).

4. Conclusion

Here, we have presented a way to study the propagation properties and its possible application for the transverse electric and transverse magnetic surface waves at the interface between a linear right-handed and a linear left-handed material. In this connection, the dispersion relations for the TE and TM surface waves have been derived and reduced for the case of linear RHM/RHM interface. These dispersion relations have been plotted numerically for the variation of various physical parameters to discuss the propagation properties of the surface waves.

The dispersion characteristics for the TE and TM waves propagating at the interface of two different right-handed media show that the surface waves propagate for the whole range of frequency but the propagation is prominent above a frequency $\omega \sim 10^{11}$ Hz. It can be seen for very small values of wave vector k below $\omega \sim 10^{11}$ Hz. This fact is useful for the microwave propagation devices e.g. filters, sensors, frequency selectors etc. Further, the dispersion curves for TE and TM wave modes have a difference in their order of magnitudes as they are separating each other continuously after $\omega \sim 10^{11}$ Hz. Therefore, the wave polarizations TE and TM can tune the device according to the desired pair of values for frequency and wave vector.

The dispersion characteristics for the TE and TM waves propagating at the interface of a RHM and a LHM show that the TM wave polarization shows continues decrease at higher frequencies which is in contrast to the dispersion characteristics of the TM polarization of RHM/RHM structure. This fact can be used as a low pass filter within the frequency band of

the left-handed material i.e. 4 to 6 GHz. Further, at lower side of the frequency band of the LHM, the dispersion curve for the TE wave polarization shows a sudden increase in amplitude and then it decreases continuously at higher values of frequency. This fact suggests that the proposed interface can be used for the designing of a band pass filter for the TE surface waves.

References

[1] E. Yablonovitch, Photonic band-gap structures, JOSA B 10 (2) (1993) 283–295.

[2] E. Istrate, E. H. Sargent, Photonic crystal heterostructures and interfaces, Reviews of modern physics 78 (2) (2006) 455.

[3] H. Benisty, C. Weisbuch, Photonic crystals, Progress in optics 49 (2006) 177.

[4] R. A. Shelby, D. R. Smith, S. Schultz, Experimental verification of a negative index of refraction, science 292 (5514) (2001) 77–79.

[5] G. V. Eleftheriades, K. G. Balmain, Negative-refraction metamaterials: fundamental principles and applications, John Wiley & Sons, 2005.

[6] V. M. Agranovich, Y. N. Gartstein, Spatial dispersion and negative refraction of light, Physics-Uspekhi 49 (10) (2006) 1029.

[7] M. A. Noginov, V. A. Podolskiy, Tutorials in metamaterials, CRC press, 2011.

[8] M. Lapine, I. V. Shadrivov, Y. S. Kivshar, Colloquium: nonlinear metamaterials, Reviews of Modern Physics 86 (3) (2014) 1093.

[9] D. R. Smith, W. J. Padilla, D. Vier, S. C. Nemat-Nasser, S. Schultz, Composite medium with simultaneously negative permeability and permittivity, Physical review letters 84 (18) (2000) 4184.

[10] R. A. Shelby, D. Smith, S. Nemat-Nasser, S. Schultz, Microwave transmission through a two-dimensional, isotropic, left-handed metamaterial, Applied Physics Letters 78 (4) (2001) 489–491.

[11] I. V. Shadrivov, A. A. Sukhorukov, Y. S. Kivshar, A. A. Zharov, A. D. Boardman, P. Egan, Nonlinear surface waves in left-handed materials, Physical Review E 69 (1) (2004) 016617.

[12] V. G. Veselago, The electrodynamics of substances with simultaneously negative values of ϵ and μ, Soviet Physics Uspekh 10 (4) (1968) 509.

[13] K. Y. Kim, Comparative analysis of guided modal properties of double-positive and double-negative metamaterial slab waveguides., Radioengineering 18 (2).

[14] J. B. Pendry, A. Holden, W. Stewart, I. Youngs, Extremely low frequency plasmons in metallic mesostructures, Physical review letters 76 (25) (1996) 4773.

[15] J. B. Pendry, A. Holden, D. Robbins, W. Stewart, Low frequency plasmons in thin-wire structures, Journal of Physics: Condensed Matter 10 (22) (1998) 4785.

[16] N. Engheta, R. W. Ziolkowski, A positive future for double-negative metamaterials, IEEE Transactions on microwave theory and techniques 53 (4) (2005) 1535–1556.

[17] N. Engheta, R. W. Ziolkowski, Metamaterials: physics and engineering explorations, John Wiley & Sons, 2006.

[18] A. Maimistov, E. Lyashko, Surface waves at the interface between a dielectric and a topological insulator, Optics and Spectroscopy 121 (2016) 635–642.

[19] M. Shen, S. Pang, J. Zheng, J. Shi, Q. Wang, Nonlinear surface polaritons in indefinite media, JOSA B 29 (2) (2012) 197–202.

[20] L. Peng, L. Duan, K. Wang, F. Gao, L. Zhang, G. Wang, Y. Yang, H. Chen, S. Zhang, Transverse photon spin of bulk electromagnetic waves in bianisotropic media, Nature Photonics 13 (12) (2019) 878–882.

[21] R. J. El-Khozondar, H. J. El-Khozondar, M. M. Shabat, Surface wave propagation at ferroelectric/mtms interface, Integrated Ferroelectrics 130 (1) (2011) 50–57.

[22] P. Markos, C. M. Soukoulis, Wave Propagation : From Electrons to Photonic Crystals and Left-Handed Materials, Princeton University Press, Princeton, 2008.

Available online at www.rpnsci.com

ISSN (P): 3006-8452, ISSN (O): 3006-8460

Research Prospects in Natural Sciences Vol. 2, Issue 2, (2024) 27–30

Research Article

Study of island height distribution for rubrene thin films deposited at different substrate temperatures using hot wall epitaxy

Kamila Rehman[a,b], Aaliya Rehman[a,*], Shaimaa M. Abdalbaqi[b], Helmut Sitter[b]

[a]*Department of Physics, Govt. M.A.O. Graduate College, Lahore 54000, Pakistan*
[b]*Institute of Semiconductor Physics, Univeristy of Linz, 4040 Linz, Austria*

Abstract

In organic thin film transistors, the hydrocarbon rubrene, due to its remarkable carrier transport capabilities has been a constant source of research and has attracted much attention. Here we have conducted a study based on the preparation and analysis of thin film deposition of rubrene on two dielectric materials, SiO_2 and mica resulting in island formation and growth. A study of island growth dependence on substrate temperatures has also been conducted. To analyze the dynamics of molecular growth of rubrene films on these substrates, we used atomic force microscopy to characterize them and studied the pattern of island growth on different substrate temperatures and substrates. In our work we observed a marked increase in island height distribution with increase in substrate temperature. This increase in island height distribution is also observed for substrates which have better sticking coefficients like mica.

Keywords:
Island growth, island count, thin films, epitaxy.

1. Introduction

One of the remarkable achievements in the field of organic electronics has been the promising results shown by field effect transistors built on single crystals of rubrene with hole mobilities as high as 15 cm^2/Vs being reached [1–6]. An average of 20 cm^2/Vs with a high of 30 cm^2/Vs hole mobility has been reported in some cases [7] which is one of the highest values recorded in similar experiments [8, 9]. However, reaching such high mobility values has its difficulties such as a reduction in measured values occurring due to oxidation when exposed to air [10]. Furthermore, since mobility values depend upon dielectric characteristics, temperature of film deposition and methods of measurement, their accuracy remains within limits [11, 12].

In contrast to the impressive results seen for single crystal form of rubrene, the results for thin films are an area of concern [6, 9, 13–18]. This is because the thin films have an amorphous form with only small regions of polycrystalline nature [19–21]. To understand the morphology of these thin films it is important to study the different stages of growth. These stages are island formation, the growth and coalescence of these islands, thin film formation and the initiation of small polycrystalline regions in these films [13–15, 20–33]. In our work presented here we have studied the initial stages of growth of rubrene thin films using inorganic substrates of mica and SiO_2 to study the dependence of island density and island growth on substrate temperatures.

2. Materials and Methods

Organic material rubrene of 98% purity was obtained from Aldrich which when treated by thermal sublimation was further purified. Rubrene was transferred to a quartz tube in the Hot Wall Epitaxy setup. Muscovite Mica substrates of size $15 \times 15 mm^2$ obtained from Segliwa GMBH were freshly hand cleaved in air and transferred to the HWE vacuum chamber. After reaching a vacuum of 10-6 mbar a preheating procedure was carried out for 15 minutes at substrate deposition temperature. This in situ heat treatment completely rids the surface of the substrates from all adsorbed materials. Rubrene was then deposited on mica (001) and freshly cleaned SiO_2 wafer (SiO_2 covered Si wafer) substrates at the vacuum of 10-6 mbar. The substrate temperatures used were 90°C and 120°C for mica while for SiO_2 it was 120°C. The source temperature for both cases was kept at 180°C while keeping the wall temperature

*Corresponding Author:
aaliya.rehman@gmail.com (Aaliya Rehman)

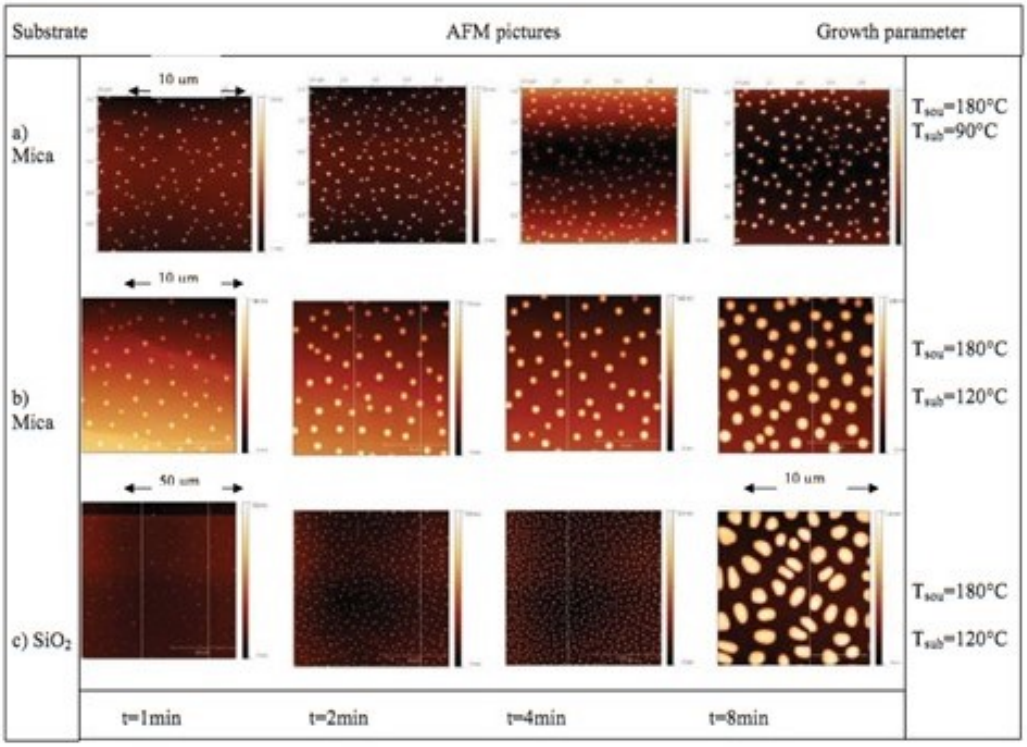

Figure 1. AFM images of rubrene grown on (a) mica surface at T_{sou} =180°C and T_{sub} = 90°C, (b) mica surface at T_{sou} =180°C and T_{sub} = 120°C and (c) SiO_2 surface at T_{sou} = 180°C and T_{sub} = 120°C, for growth times 1, 2, 4 and 8 minutes. The magnifications of images are (a) $10 \times 10\mu m^2$, (b) $10 \times 10\mu m^2$ and (c) $50 \times 50\mu m^2$.

also at 180°C. Growth time for the samples was 1, 2, 4 and 8 minutes. Morphology studies were carried out by obtaining atomic force microscopy (AFM) images of the deposited organic thin films in the tapping mode of Digital Instruments Dimension 3100 microscope, where a SiC tip was used on areas of $10 \times 10\mu m^2$ and $50 \times 50\mu m^2$. Fig.1 shows these AFM scans of rubrene deposited on muscovite mica and SiO_2 substrates. These series of AFM scans were analysed in the following way. The island density was evaluated by counting the number of grains per $10 \times 10\mu m^2$. By analysing a representative number of cross sections of the islands formed, the average height of these islands was evaluated which was then used for island height distribution calculations.

3. Results and Discussion

Rubrene was deposited on mica (001) and SiO_2 wafer substrates by using hot wall epitaxy at a vacuum of 10-6 mbar. The substrate temperatures used were 90°C and 120°C for mica while for SiO_2 it was 120°C. The source temperature for both cases was kept at 180°C. Morphology was assessed by getting the AFM scans. Fig.1 shows these AFM scans of rubrene deposited on muscovite mica and SiO_2 substrates.

Fig.2 shows that increase in substrate temperatures results in increased island heights while island count decreases for higher substrate temperatures. This can be understood by the different diffusion lengths of rubrene molecules. At high substrate

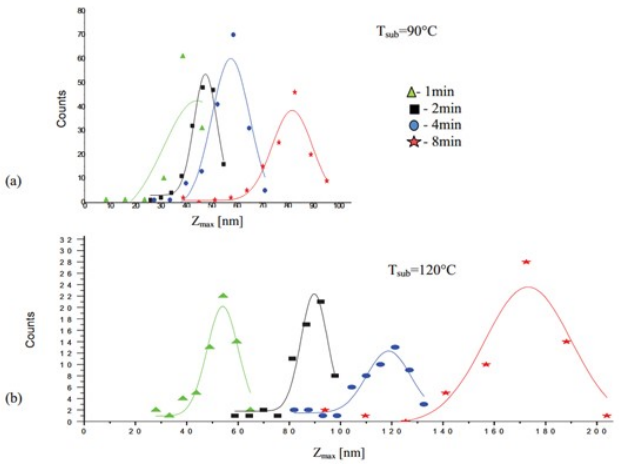

Figure 2. The comparison of the island height distribution Z_{max} for samples grown on mica at substrate temperature of (a) 90°C and (b) 120°C, and source temperature of 180°C.

temperatures diffusion length is in the range of the average island distance, so each impinging molecule can reach its optimum position at the edge of an island. On the other hand, at lower substrate temperatures the diffusion length of the impinging rubrene molecules is smaller and consequently in the beginning of growth, new islands are formed. This continues until the density of islands reaches a limit at which all molecules can reach the islands to be incorporated and consequently a satura-

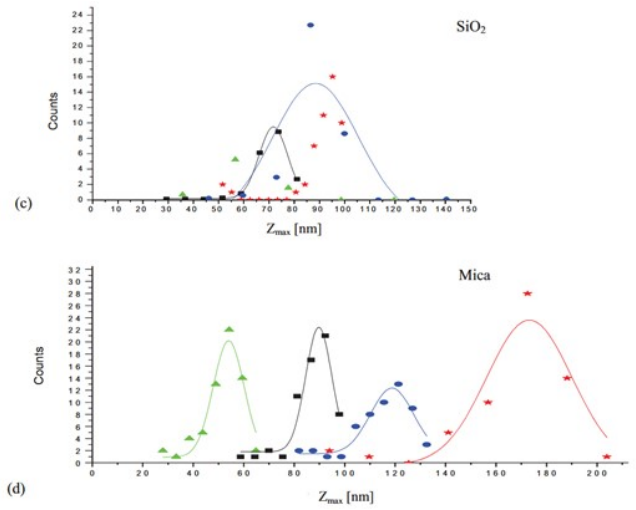

Figure 3. Comparison of the island height distribution for rubrene samples grown on mica (c) and SiO_2 (d) at substrate temperature of 120°C and source temperature of 180°C.

tion at higher island density was observed for lower substrate temperature.

A comparison is shown in Fig.3 for samples grown at source temperatures of 180°C and substrate temperature of 120°C but on different substrates of SiO_2 and mica. The corresponding AFM pictures are shown in Fig.1 b) and c). Due to a smaller sticking coefficient of rubrene on SiO_2, by using the same evaluation process as described above, we can see why the island height distribution for SiO_2 is lower as compared to mica for the same substrate temperature.

4. Conclusion

We have investigated the island height distribution of rubrene deposited on two different substrates by using the method of Hot-Wall-Epitaxy at different substrate temperatures. Keeping the deposition rate constant for all our experiments, we see that the island height distribution shows dependence on the substrate temperatures, increasing as we reach higher temperatures. Furthermore, sticking coefficients of substrates play an important role in the growth process and must be taken into consideration when choosing the optimum substrate temperatures for film growth.

References

[1] K. A. McGarry, W. Xie, C. Sutton, C. Risko, Y. Wu, V. G. Young Jr, J.-L. Brédas, C. D. Frisbie, C. J. Douglas, Rubrene-based single-crystal organic semiconductors: Synthesis, electronic structure, and charge-transport properties, Chemistry of Materials 25 (11) (2013) 2254–2263.

[2] W. Xie, P. L. Prabhumirashi, Y. Nakayama, K. A. McGarry, M. L. Geier, Y. Uragami, K. Mase, C. J. Douglas, H. Ishii, M. C. Hersam, et al., Utilizing carbon nanotube electrodes to improve charge injection and transport in bis (trifluoromethyl)-dimethyl-rubrene ambipolar single crystal transistors, ACS nano 7 (11) (2013) 10245–10256.

[3] P. S. Jo, D. T. Duong, J. Park, R. Sinclair, A. Salleo, Control of rubrene polymorphs via polymer binders: Applications in organic field-effect transistors, Chemistry of Materials 27 (11) (2015) 3979–3987.

[4] C. Wang, H. Dong, W. Hu, Y. Liu, D. Zhu, Semiconducting π-conjugated systems in field-effect transistors: a material odyssey of organic electronics, Chemical reviews 112 (4) (2012) 2208–2267.

[5] M. A. Reyes-Martinez, A. J. Crosby, A. L. Briseno, Rubrene crystal field-effect mobility modulation via conducting channel wrinkling, Nature communications 6 (1) (2015) 6948.

[6] V. C. Sundar, J. Zaumseil, V. Podzorov, E. Menard, R. L. Willett, T. Someya, M. E. Gershenson, J. A. Rogers, Elastomeric transistor stamps: reversible probing of charge transport in organic crystals, Science 303 (5664) (2004) 1644–1646.

[7] J. Nitta, K. Miwa, N. Komiya, E. Annese, J. Fujii, S. Ono, K. Sakamoto, The actual electronic band structure of a rubrene single crystal, Scientific Reports 9 (1) (2019) 9645.

[8] W. Xie, K. A. McGarry, F. Liu, Y. Wu, P. P. Ruden, C. J. Douglas, C. D. Frisbie, High-mobility transistors based on single crystals of isotopically substituted rubrene-d 28, The Journal of Physical Chemistry C 117 (22) (2013) 11522–11529.

[9] J. Takeya, M. Yamagishi, Y. Tominari, R. Hirahara, Y. Nakazawa, T. Nishikawa, T. Kawase, T. Shimoda, S. Ogawa, Very high-mobility organic single-crystal transistors with in-crystal conduction channels, Applied Physics Letters 90 (10).

[10] H. Ma, N. Liu, J.-D. Huang, A dft study on the electronic structures and conducting properties of rubrene and its derivatives in organic field-effect transistors, Scientific reports 7 (1) (2017) 331.

[11] V. Coropceanu, J. Cornil, D. A. da Silva Filho, Y. Olivier, R. Silbey, J.-L. Brédas, Charge transport in organic semiconductors, Chemical reviews 107 (4) (2007) 926–952.

[12] C. Kim, A. Facchetti, T. J. Marks, Gate dielectric microstructural control of pentacene film growth mode and field-effect transistor performance, Advanced Materials 19 (18) (2007) 2561–2566.

[13] S.-W. Park, J. M. Hwang, J.-M. Choi, D. Hwang, M. Oh, J. H. Kim, S. Im, Rubrene thin-film transistors with crystalline and amorphous channels, Applied physics letters 90 (15).

[14] S.-W. Park, S. Jeong, J.-M. Choi, J. M. Hwang, J. H. Kim, S. Im, Rubrene polycrystalline transistor channel achieved through in situ vacuum annealing, Applied Physics Letters 91 (3).

[15] C. Hsu, J. Deng, C. Staddon, P. Beton, Growth front nucleation of rubrene thin films for high mobility organic transistors, applied physics letters 91 (19).

[16] V. Podzorov, V. Pudalov, M. Gershenson, Field-effect transistors on rubrene single crystals with parylene gate insulator, Applied physics letters 82 (11) (2003) 1739–1741.

[17] C. Goldmann, S. Haas, C. Krellner, K. Pernstich, D. Gundlach, B. Batlogg, Hole mobility in organic single crystals measured by a "flip-crystal" field-effect technique, Journal of Applied Physics 96 (4) (2004) 2080–2086.

[18] E. Menard, V. Podzorov, S.-H. Hur, A. Gaur, M. E. Gershenson, J. A. Rogers, High-performance n-and p-type single-crystal organic transistors with free-space gate dielectrics, Advanced materials 16 (23-24) (2004) 2097–2101.

[19] H. Klauk, M. Halik, U. Zschieschang, G. Schmid, W. Radlik, W. Weber, High-mobility polymer gate dielectric pentacene thin film transistors, Journal of Applied Physics 92 (9) (2002) 5259–5263.

[20] C. Sheraw, L. Zhou, J. Huang, D. Gundlach, T. Jackson, M. Kane, I. Hill, M. Hammond, J. Campi, B. Greening, et al., Organic thin-film transistor-driven polymer-dispersed liquid crystal displays on flexible polymeric substrates, Applied physics letters 80 (6) (2002) 1088–1090.

[21] D. Käfer, L. Ruppel, G. Witte, C. Wöll, Role of molecular conformations in rubrene thin film growth, Physical review letters 95 (16) (2005) 166602.

[22] M. Campione, Rubrene heteroepitaxial nanostructures with unique orientation, The Journal of Physical Chemistry C 112 (42) (2008) 16178–16181.

[23] M. Haemori, J. Yamaguchi, S. Yaginuma, K. Itaka, H. Koinuma, Fabrication of highly oriented rubrene thin films by the use of atomically finished substrate and pentacene buffer layer, Japanese journal of applied physics 44 (6R) (2005) 3740.

[24] D. Käfer, G. Witte, Growth of crystalline rubrene films with enhanced stability, Physical Chemistry Chemical Physics 7 (15) (2005) 2850–2853.

[25] Y. Chen, I. Shih, High mobility organic thin film transistors based on monocrystalline rubrene films grown by low pressure hot wall deposition,

Applied Physics Letters 94 (8).

[26] Y. Luo, M. Brun, P. Rannou, B. Grevin, Growth of rubrene thin film, spherulites and nanowires on sio2, physica status solidi (a) 204 (6) (2007) 1851–1855.

[27] P. R. Ribić, G. Bratina, Ripening of rubrene islands, The Journal of Physical Chemistry C 111 (50) (2007) 18558–18562.

[28] S. Kowarik, A. Gerlach, S. Sellner, F. Schreiber, J. Pflaum, L. Cavalcanti, O. Konovalov, Anomalous roughness evolution of rubrene thin films observed in real time during growth, Physical Chemistry Chemical Physics 8 (15) (2006) 1834–1836.

[29] G. Hlawacek, S. Abd-al Baqi, X. Ming He, H. Sitter, C. Teichert, Rubrene on mica: from the early growth stage to late crystallization, Interface Controlled Organic Thin Films (2009) 55–60.

[30] L. Gránásy, T. Pusztai, T. Börzsönyi, J. A. Warren, J. F. Douglas, A general mechanism of polycrystalline growth, Nature Materials 3 (9) (2004) 645–650.

[31] M. Brinkmann, S. Graff, F. Biscarini, Mechanism of nonrandom pattern formation of polar-conjugated molecules in a partial wetting regime, Physical review B 66 (16) (2002) 165430.

[32] Y. Kato, S. Iba, R. Teramoto, T. Sekitani, T. Someya, H. Kawaguchi, T. Sakurai, High mobility of pentacene field-effect transistors with polyimide gate dielectric layers, Applied physics letters 84 (19) (2004) 3789–3791.

[33] U. Stadlober, B Haas, A. Maresch, H Haase, Semiconductors ii: Surfaces, interfaces, microstructures, and related topics-growth model of pentacene on inorganic and organic dielectrics based on scaling and rate-equation theory, Physical Review-Section B-Condensed Matter 74 (16) (2006) 165302–165302.

RESEARCH PROSPECTS IN NATURAL SCIENCES IS A BIANNUAL SCHOLARLY PERIODICAL ISSUED BY GOVT GRADUATE COLLEGE TOWNSHIP, LAHORE, THAT STRIVES TO DISSEMINATE THE EMPIRICAL WORK OF RESEARCHERS WORLDWIDE THROUGH SCRUTINIZED RESEARCH ARTICLES, WITH THE INTENTION OF ESTABLISHING ITSELF AS A LEADING FORUM FOR TOP-NOTCH RESEARCH PUBLICATIONS AND ENDORSING LEARNED TREATISES AND RESEARCH PAPERS.

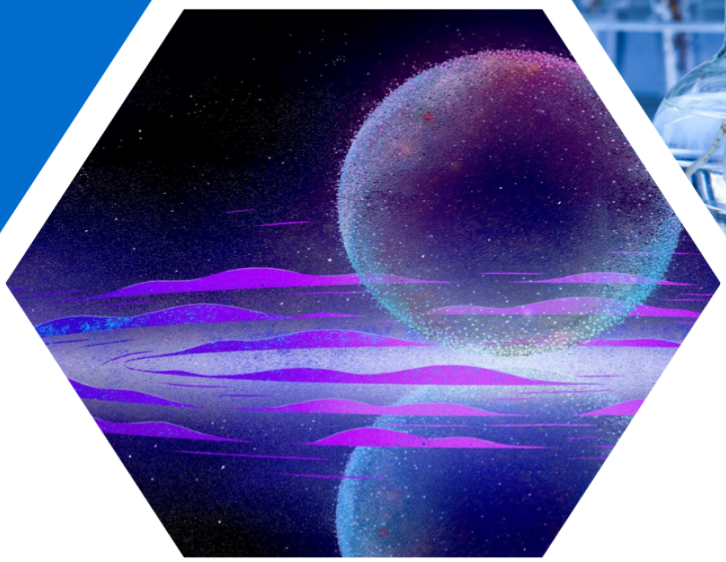

GOVERNMENT GRADUATE COLLEGE, TOWNSHIP, LAHORE